Multi-Frequency Control of Single-Stage Converters using High-Frequency Isolation Transformers

by

Juan Reynaldo Zuniga Gutierrez

A thesis submitted in partial fulfillment of the requirements for the degree of

Master of Science

in

Energy Systems

Department of Electrical and Computer Engineering
University of Alberta

UNIVERSITY OF ALBERTA

Abstract

Faculty of Graduate Studies and Research
Department of Electrical and Computer Engineering
Master of Science

Multi-Frequency Control of Single-Stage Converters using High-Frequency Isolation Transformers

by Juan Reynaldo Zuniga Gutierrez

Galvanic isolation using transformers is an important feature of many power converters, providing additional safety by separating the ground potential of two or more sections of an electrical system. High-frequency (HF) transformers increase the power density of converters by reducing the core size and weight. A further increase in power density can be achieved by using a single power conversion stage. Two single-stage power converter systems offering HF isolation are presented: a dc to ac converter and a multiport topology. The converters take advantage of the differential (DM) and common-mode (CM) currents that can be driven using center-tapped transformers connected to dual inverters. The DM currents are generated as HF three-phase sinusoidal currents to achieve power control through the transformers, introducing a straightforward alternative approach to the conventional dual active bridge (DAB) concept, where square-wave voltages are phase shifted to control HF transformer power transfer. The CM currents are generated as low-frequency (LF) currents for ac grid power exchange. A multi-frequency pulse-

width modulation (PWM) scheme is employed to generate these current components. Independent control of HF transformer power and LF ac power can be realized using well-established control techniques, such as dq-frame current control, simplifying the implementation of the converter concept. Both converter systems are experimentally validated, showing that decoupled control of ac grid power and HF transformer power can be attained. Moreover, the converters are shown to have reduced ac output filtering requirements than two-level voltage-source converters. The multiport converter concept is among a very limited number of single-stage converters offering HF isolation that can realize ac-ac power conversion.

Preface

The research work presented in this thesis has led to two publications in IEEE:

i) The paper "Bidirectional DC-AC Converter Using a High-Frequency Transformer with Multi-Frequency Decoupled Power Control" authored by Juan Zuniga, Marius Takongmo, Chatumal Perera, Vishwa Perera and John Salmon has been accepted for publication in IEEE Energy Conversion Congress and Exposition (ECCE) 2021.

ii) The paper "Multiport Converter with High-Frequency Isolation for Asynchronous AC Ports" authored by Juan Zuniga, Marius Takongmo, Chatumal Perera and John Salmon has been submitted for publication in IEEE Transactions on Power Electronics as a letter.

The work of the first publication is presented with additional details in chapter 2, while chapter 3 expands on the work presented in the second publication. I was in charge of the preparation and evaluation of the simulation models, as well as setting up the experimental system and running the tests, the collection and analysis of experimental data and writing the drafts that preceded the aforementioned publications. Dr. John Salmon supervised the development of the research, contributed to the creation of both converter concepts and was the main editor of the published material. Chatumal Perera originally proposed the converter principle of operation and control strategy. Marius Takongmo designed and manufactured the high-frequency transformers and, together with Vishwa Perera, helped in the execution of several experimental tests. The experimental hardware and laboratory equipment were supplied by Dr. John Salmon.

I dedicate this work to my mother, my brothers, my father, and Karla...

Thank you for being with me, so far, yet so close...

Acknowledgements

I would like to thank Dr. John Salmon, first and foremost, for giving me the opportunity to join his research group. Without his interest in me as an MSc student, I probably would not have embarked on the adventure that studying at the University of Alberta has been. He has also been an excellent and unorthodox supervisor. I have truly enjoyed being part of his group. I also wish to thank Dr. Gregory Kish, who referred me to Dr. Salmon in the early stages of my application process.

I want my mother to know that I am very grateful for giving me the foundations that have supported my achievements. I know she has endured many hardships in life for the sheer love to her sons, and for that I am forever indebted. I want to thank my brothers, Alex, and Tony, for being there; even in the distance you make me feel so much younger. I want to thank my father for being always present in my life, throughout which, he has shared his wisdom and unique view of the world with me and has always been there when I have needed him. To my stepfather, who is no longer among us: thank you for your hard work and for looking out for us. I also want to express my sincere gratitude to my partner Karla, for being the best moral support throughout all my endeavors and for being by my side all these years: the best is yet to come.

I have been very fortunate to have joined this research group, as I have been able to meet a group of colleagues who, beyond that, I consider my friends. I want to thank Vishwa, Chatumal, Marius and Chenhui for making this graduate program a great experience. Special thanks go to Chatumal, for sharing his knowledge and helping me speed up the learning curve; to Vishwa for his friendship and for helping me with the early experimental stages and to Marius, who contributed greatly to the design and construction of the magnetics.

I would like to acknowledge the Natural Sciences and Engineering Research Council of Canada (NSERC) whose funding has made possible the use of the laboratory equipment and material used for this work. I want to express my gratitude to the Sponsored Student Program for their valuable support at the very early stages of my application and to the University of Alberta, for fostering a diverse and supportive community. Lastly, I want to thank the National Council of Science and Technology (CONACYT) of Mexico for their financial support; without it I would not be here.

Contents

List of Tables

List of Figures

Abbreviations

2-L	**T**wo-**L**evel
CM	**C**ommon **M**ode
DAB	**D**ual **A**ctive **B**ridge
DFIG	**D**oubly-**F**ed **I**nduction **G**enerator
DM	**D**ifferential **M**ode
DVR	**D**ynamic **V**oltage **R**estorer
EMI	**E**lectro**m**agnetic **I**nterference
EV	**E**lectric **V**ehicle
HF	**H**igh **F**requency
HVDC	**H**igh-**V**oltage **D**irect **C**urrent
KVL	**K**irchhoff's **V**oltage **L**aw
LF	**L**ow **F**requency
MF	**M**edium **F**requency
MMC	**M**odular **M**ultilevel **C**onverter
MVAC	**M**edium-**V**oltage **A**lternating **C**urrent
MVDC	**M**edium-**V**oltage **D**irect **C**urrent
PI	**P**roportional **I**ntegral
PLL	**P**hase-**L**ocked **L**oop
PMSG	**P**ermanent **M**agnet **S**ynchronous **G**enerator
PV	**P**hoto**v**oltaic
PWM	**P**ulse-**W**idth **M**odulation
RL	**R**esistive-**I**nductive
SPWM	**S**inusoidal **PWM**
SST	**S**olid-**S**tate **T**ransformer
STATCOM	**Stat**ic **Com**pensator
VFD	**V**ariable **F**requency **D**rive
VSC	**V**oltage-**S**ource **C**onverter
WECS	**W**ind **E**nergy **C**onversion **S**ystem

Chapter 1

Grid-Connected High-Frequency Isolated Converters

Transformers are a widely employed passive element in power converters. They offer galvanic separation between two or more sections of an electrical system, can prevent dc components from entering ac power systems and allow to easily step up or step down ac voltages. They can also be one of the heaviest and bulkiest components in electrical systems; especially when operated at low frequencies, such as the grid frequency. For this reason, it is common to operate transformers in power converters at higher frequencies, as they can be made smaller and lighter. Several power converters that interact with ac systems, such as rectifiers, inverters, ac-ac converters, and some multiport converters, leverage high-frequency (HF) transformers to provide the aforementioned benefits while achieving high power density.

Two power converter systems are presented that offer high power density by employing HF transformers and achieving single-stage power processing, with a unique control approach. As it relates to the converter systems presented, the context where dc-ac, ac-ac, and multiport converters are applied is briefly presented here, followed by a discussion of two different solutions to realize HF isolation[1]. Finally, the objective, structure and contributions of the thesis are presented.

[1] For the purposes of this thesis HF isolation refers to the inclusion of HF transformers, which can also attain voltage step up and step down. For simplicity, a 1:1 transformation ratio is used in the converter concepts presented, without loss of generality.

1.1 DC-AC Converters

With the increasingly pressing need to move away from conventional carbon-based energy sources, contemporary power grids are integrating a growing amount of dc sources and storage elements, such as photovoltaic (PV) systems and batteries in electric vehicles (EV), extending the presence of inverters and rectifiers of diverse power ratings in the modern power system. Moreover, large-scale integration of wind generators is prompting the development of high-voltage direct current (HVDC) power systems, where bidirectional dc to ac conversion at power levels of several MW is required. In addition to these trending applications, dc-ac converters have been widely employed in all sorts of electronic devices and appliances, as well as in high-power industrial settings, like static compensators (STATCOM) and rectifiers for electric arc furnaces.

In most applications, it is desirable to include transformers for galvanic isolation, dc voltage blocking, and voltage step up/step down. For instance, galvanic isolation in PV systems has historically been required by many jurisdictions [1, pp. 16-18] to ensure that no dc voltages are fed to the grid. This requirement has been met by PV inverters using low-frequency (LF) transformers, HF transformers or by providing additional safety features in non-isolated inverters [2, pp. 123-127][2]. Similarly, in EV charging stations and built-in on-board chargers, the inclusion of isolation transformers in the rectifier circuit is required to provide safety by separating the ground reference of the grid side and the vehicle side of the converter [3]. Therefore, the inclusion of transformers is a common practice in dc-ac converters.

1.2 AC-AC and Multiport Converters

The conversion of ac voltages of different frequencies and amplitudes is a common process in industrial settings. Practically, wherever variable frequency drives (VFD) are employed, ac-ac conversion takes place, taking power from the grid (or generators), converting it to dc and then inverting it back to variable frequency ac. VFDs find application in almost all industrial sectors, ranging from mining operations, oil and gas, metal processing to food and beverage production,

[2] Non-isolated (also known as *transformerless*) inverters have become more popular in recent years as they offer reduced size and weight and increased efficiency compared to transformer-based solutions.

water treatment facilities, marine propulsion, etcetera [4]. In wind energy generation, back-to-back converters have become the norm [5, pp. 9-11], as they allow variable-speed operation of wind turbines, maximizing power extraction from the wind. Similar ac-ac converter structures are used in substations that interconnect asynchronous grids [6, p. 805][3]. These ac-ac converters are classified as converters with dc-link energy storage because they have an intermediate energy storage element [7].

AC-AC conversion is commonly associated to direct power converters, such as matrix converters and their variants[4]. Matrix converters allow ac-ac conversion without using intermediate energy storage elements [7]. Although they are not as widespread as conventional solutions (e.g., pulse-width modulated VFDs) due to their performance limitations [8], they have found applications driving low-speed synchronous motors of several MW. For instance, in cement mills and cruise ship propulsion motors [6, p. 606]. Recent research has presented matrix converters for applications such as induction heating for metal hardening [9], wireless charging [10], as dynamic voltage restorers (DVR) for grid voltage regulation [11] and for wind energy generation [12].

Most of the cited applications involve the use of transformers in the process of converting ac to ac. In wind farms, for example, transformers are used to step up the output of the converter to a higher voltage [5, p. 7]. This applies to wind generators using both full and partial-rated converter topologies, such as permanent magnet synchronous generators (PMSG) and doubly-fed induction generators (DFIG), respectively [5, pp. 8-10]. In back-to-back converter stations, transformers are necessary to match the voltage of the converters and the ac transmission systems [13]. Hence, these applications can benefit from ac-ac converters that integrate transformers in their structure.

An application for ac-ac isolated converters that has drawn major research interest is the solid-state transformer (SST), which is seen as the candidate technology to replace conventional passive transformers in future power grids, offering advanced power support features, reduced size and weight, modularity, and flexibility [14]. Moreover, it is projected that future power grids will

[3] Converter stations such as Al-Fadhili in Saudi Arabia [13] and Garabi in Brazil [46], realize ac-ac conversion between ac power systems that operate at different frequencies utilizing back-to-back converters.

[4] A comprehensive review of ac-ac converter topologies can be found in [7] and [45].

accommodate a variety of ac and dc sources, loads and storage elements [15], [16], as the energy mix shifts from traditional carbon-based sources to renewable energy sources, and as power systems become more flexible to incorporate a larger participation of these variable power sources. In this scenario, SSTs can provide more than ac-ac conversion and advanced functionalities; they can also serve as multiport converters. Multiport converters have three or more power ports, whether dc or ac. They combine the functionality of multiple separate power converters, each interfaced with different power ports, into a single unit [17]; thus, allowing sources, loads and storage elements of different electrical characteristics to interact with each other and regulating the power flow between them.

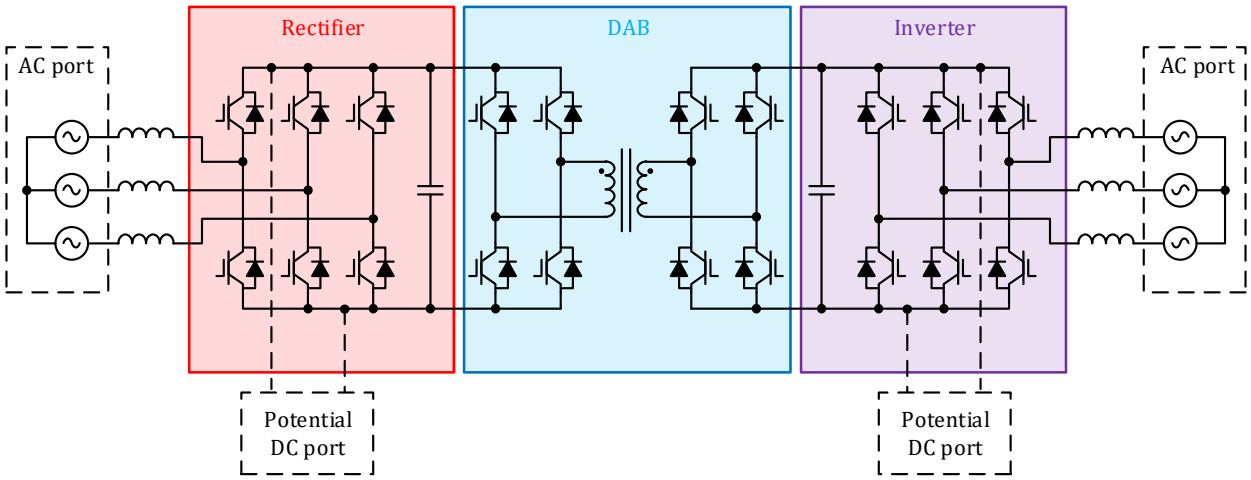

Figure 1.1. Conventional solid-state transformer topology showing potential dc ports.

As an example, a conventional three-stage SST solution [18] that performs voltage step up and step down can work as a multiport converter if the dc links of the front and back-end voltage-source converters (VSC; rectifier and inverter in Figure 1.1, respectively) are used to connect two dc ports. Such a converter can be used in a hybrid ac-dc grid, connecting to medium-voltage ac (MVAC) and dc (MVDC) grids on the high-voltage side, and integrating battery storage and local dc and ac networks in the low-voltage side [19]. Wind generators can also benefit from isolated multiport converters, allowing to integrate the transformer and battery storage within the same converter unit that performs ac-ac conversion [20]. Because of this, isolated multiport converters are a topic that has been widely investigated in recent literature.

1.3 High-Frequency Isolation

Most power systems around the world operate at frequencies of 50 and 60 Hz. The establishment of these frequencies as the standard grid frequency dates back to the early 20th century [21], with some systems operating at different frequencies used in rail traction (16.7 Hz) [21] and aircraft [22], for example. Power transformers are, therefore, designed to operate at 50 or 60 Hz, depending on the ac system they are connected to. They are an essential element of ac systems, allowing to easily increase or decrease the ac voltage for high-efficiency transmission and distribution. Their simplicity, ruggedness, low maintenance requirements and easy manufacturing process has allowed them to become a ubiquitous artifact. One of their main drawbacks, however, is their high weight and volume. Transformers are not easy to handle, transport and install, especially at increasing power ratings (Figure 1.2).

Figure 1.2. Delivery of a 45-kVA 1.2-ton auxiliary transformer (left) and a 40-MVA 38-ton step-up transformer (right) for a PV power plant (photographs taken by author).

It is for this reason that most isolated power converters employ HF transformers instead of LF designs. To illustrate the difference in size and weight of both design options, consider the equation of flux ϕ induced in a transformer core when a sinusoidal voltage $v(t)$ of amplitude $\hat{v}$ and angular frequency ω is applied to its primary winding, [23, p. 81]:

$$\phi = \frac{1}{N}\int \hat{v}\cos\omega t\, dt \tag{1}$$

Where N is the number of turns in the primary (assumed the same for the secondary). Knowing that the flux density B is related to the core cross-sectional area A by $B = \phi/A$, (1) can be written as

$$B = \frac{1}{NA}\int \hat{v}\cos\omega t\, dt \tag{2}$$

Expanding the integral yields

$$B = \frac{\hat{v}}{\omega NA}\sin\omega t \tag{3}$$

The cross-sectional area of the core can be expressed as

$$A = \frac{\hat{v}}{\omega NB}\sin\omega t \tag{4}$$

Therefore, if we have two transformers made of the same core material, the flux density that can flow through the cores without saturating them is the same for both, making B a constant value below the saturation limit of the core material (e.g., 1.56 T for the 2605SA1 Metglas amorphous Alloy [24]). Using the same number of turns N and applying two sinusoidal voltages of the same amplitude $\hat{v}$ but different frequencies, ω and 10ω, to both cores, the cross-sectional area required to avoid transformer saturation is ten times smaller for the core operating at 10ω. For example, if the first transformer has a cross-sectional area of 21 cm^2, using the 2605SA1 Metglas amorphous Alloy, its total mass would be of about 6 kg, taking over 1,300 cm^3 of space. Now, if the cross-sectional area of the second transformer can be made ten times smaller by operating at a higher frequency, a transformer core of less than 300 g could be chosen, taking up only 5% of the volume of the first transformer, Figure 1.3.

From the previous example, the advantage of using HF over LF transformers in power converters is evident. Nevertheless, ac grid systems run at lower frequencies. If the converters are to be connected to an ac grid, they have to generate power at the same frequency as the grid. Therefore, to attain the benefit of reduced overall converter size and weight, they must operate their isolation transformer at HF, while providing a grid-compatible LF power output. There are two basic approaches to achieve these objectives: using several cascaded converter stages (Figure 1.1) or designing a converter system that can fulfill these objectives using a single conversion stage.

The contribution of this thesis is, precisely, to introduce converters that employ HF currents for electrical transformer isolation and LF currents to exchange power to the grid.

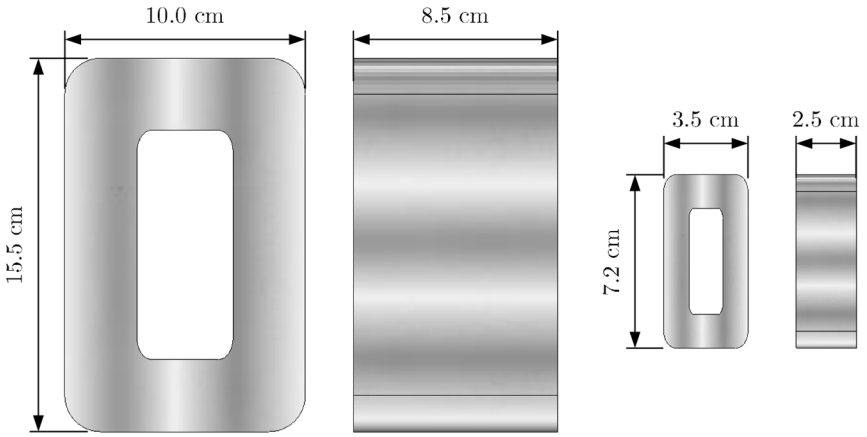

Frequency: ω
Mass: 6,000 g
Volume: 1,317 cm^3

Frequency: 10ω
Mass: 280 g
Volume: 63 cm^3

Figure 1.3. Example of cores for transformers designed to operate at two different frequencies (mass and dimensions from [25]; the volume considers the core approximated by a rectangular parallelepiped).

The focus of the following subsections is to provide a review of some of the most relevant circuits that use either of both approaches. With this purpose in mind, the reviewed converters are summarized in Table 1.1, showing their circuit diagram and some of the key characteristics to ease direct comparison. Advantages and drawbacks of the different approaches and topologies are then discussed to give the reader context before the benefits of the converters presented in this thesis are introduced.

Table 1.1 Comparison of converters with HF isolation.

Reference	Total ports	AC ports	DC ports	Bidirectional	Resonant	Single-stage	Phases	Active switches [a]	Exp. power (kW)	Center-tapped	Frequency type [b]	Frequency (kHz)	Power transfer control	Topology
DC-AC														
[26]	2	1	1	✓	X	X	3	14	10	X	f_{sw}	20	Phase shift	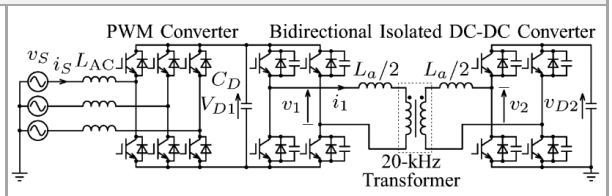
[27]	2	1	1	✓	X	✓	1	8	-	X	f_{sw}	50	Phase shift	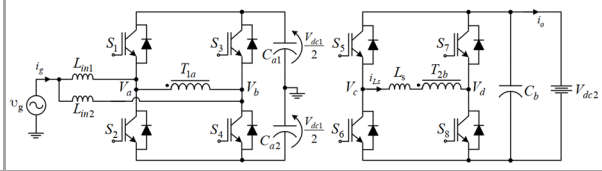
[28]	2	1	1	✓	X	✓	3	24	5.0	✓	f_{sw}	50	Phase shift	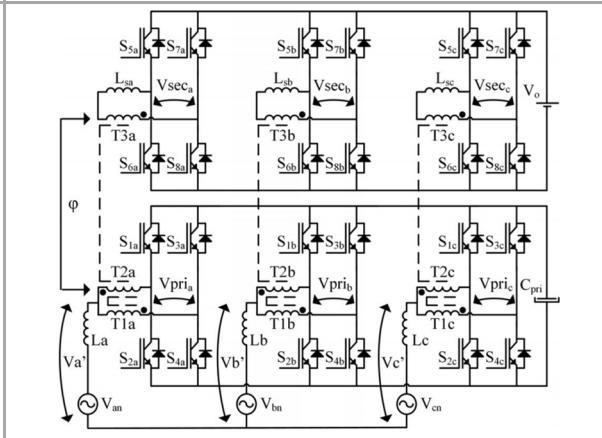
[29]	2	1	1	✓	X	✓	1	8	0.3	X	f_{sw}	25	Phase shift	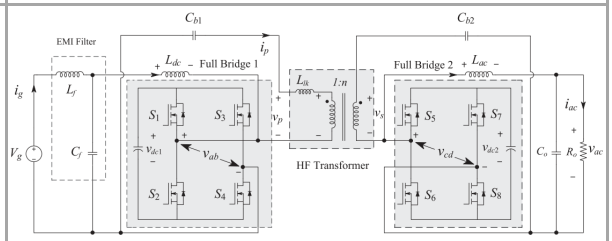
[30]	2	1	1	✓	✓	✓	1	12	-	X	RF	30	Resonance	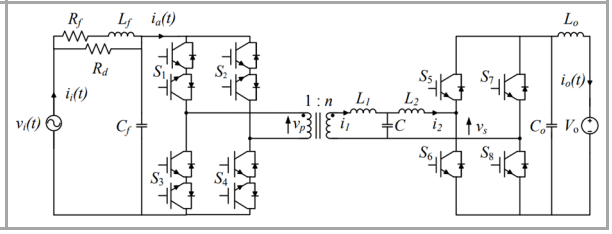

[31]	2	1	1	✓	✓	✓	1	8	-	X	RF	60	Resonance
This work	2	1	1	✓	X	✓	3	24	1.4	✓	Sine	2	HF sine
Multiport													
[18]	4	2	2 [c]	✓	X	X	3	20	2	X	f_{sw}	10	Phase-shift
[32]	4	2	2	✓	✓	X	3	26	0.2	X	RF	2	Resonance
[33]	3	2	1	✓	X	X	3	42	1.2	X	Sq. wave	0.6	Phase shift

[34]	4	0	4	✓	X	✓	DC	8	1.5	✓	f_{sw}	40	Phase shift
[35]	4	1	3	✓	X	✓	3	24	6.0	✓	f_{sw}	50	Phase shift
[36]	3	1	2	✓	X	✓	1	8	0.2	X	f_{sw}	50	Phase shift
[37]	3	1	2	X	X	✓	3	6	1.3	X	$2f_{sw}$	100	Non regulated
This work	4	2	2	✓	X	✓	3	24	1.3	✓	Sine	2	HF sine

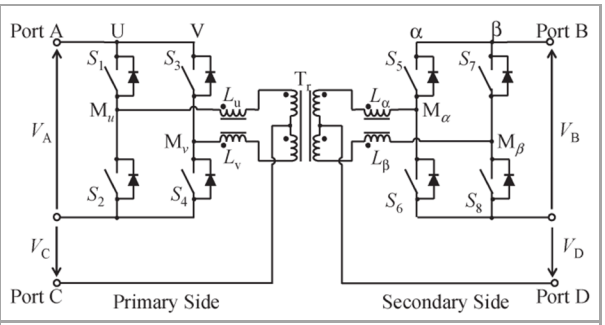

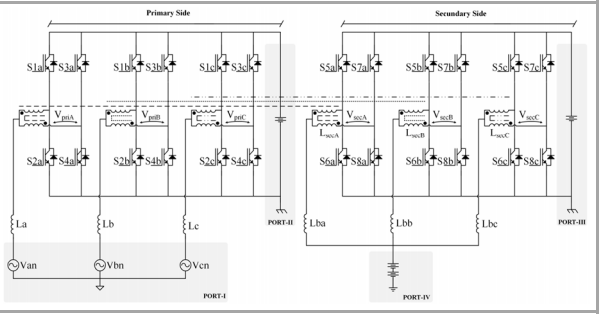

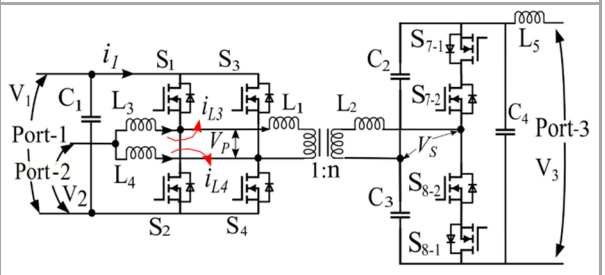

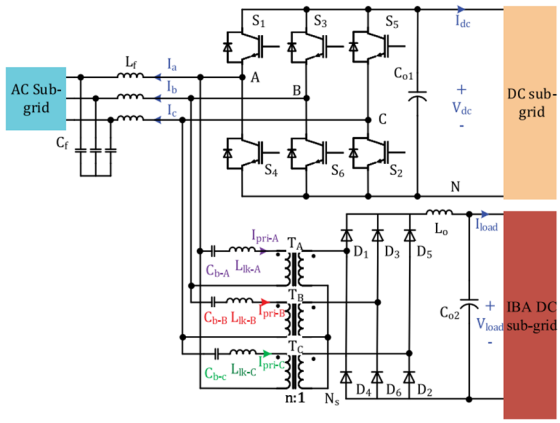

(See Figure 3.1)

[a] The converters in [32] and [33] use multiple series-stacked power modules; to ease comparison, a single level is assumed here.

[b] f_{sw}: switching frequency; RF: resonant frequency; Sine: sine-wave modulation; Sq. wave: Square-wave modulation.

[c] The converter in [18] can have two dc ports if the low and high-voltage dc links are considered.

1.3.1 Multi-Stage Solutions

A simple solution to provide HF isolation while generating grid-compatible power is to connect multiple converter stages in sequence. This is a common solution that has been widely applied in industry [2, pp. 124-125], [38], [39]. The three-stage SST [18] shown in Figure 1.1 is an example of a multi-stage ac-ac converter. It comprises a rectifier (ac to dc stage), followed by a single-phase dual active bridge (DAB; dc to dc stage), and an inverter (dc to ac stage). A similar solution can be used to achieve isolated dc to ac conversion, using only a DAB (dc to dc) stage and an inverter (dc to ac) stage, [26], Table 1.1. The DAB stage allows to use a HF transformer design.

Although dc to dc converter topologies like flyback or push-pull allow to use a HF transformer too, DABs are one of the most popular dc to dc converter stages used to provide HF transformer isolation [40]. Some of the key benefits of DAB converters are:

1. Their ability to operate at the switching frequency, driving the size and weight of transformers to a minimum.
2. Their forthright control principle, using the phase shift between the square-wave voltages applied on both sides of the transformer to send or receive HF power.
3. The possibility to use soft switching to reduce switching losses.

On the other hand, some drawbacks inherent to DABs are:

1. The relation between power and the control variable, which is the phase-shift angle, is nonlinear, adding complexity to the derivation of controllers.
2. Although power transfer across the transformer can be achieved by simply increasing the phase shift between the square-wave voltages applied on both sides, the presence of reactive power in the windings also increases. Hence, a limited range of phase-shift angles is preferred [41, pp. 107-108], e.g., less than 40°.

In regard to multiport converters, the three-stage SST (Figure 1.1) can provide additional dc ports using the dc links on both sides of the DAB, supporting two ac ports and two dc ports, [18], Table 1.1. Another solution that supplies a similar port count uses a modular multilevel converter (MMC) as an interface between a three-phase MVAC grid and an MVDC system, [32], Table 1.1. A multi-frequency modulation scheme using a medium-frequency (MF) square-wave superposed on a LF sinusoidal signal is used. This scheme generates the MVAC-side voltages and excites the

resonant branches, producing MF resonant currents that convey power across MF step-down transformers. Two full-bridge converters (each for the upper and lower-arm transformers) on the secondary side of these transformers convert the MF ac voltages to LF dc voltages; hence, providing a LF dc port. An additional two-level (2-L) VSC stage is used to connect to a LF three-phase ac system. The converter is interesting, as it employs multi-frequency signals for decoupled control of different ports. Even so, it is evident that the component count is high (e.g., capacitors, inductors, and switches), due to the existence of multiple power processing stages.

Another isolated multiport converter using the multi-stage approach has been suggested for wind energy generation, [33], Table 1.1. It uses series-stacked single-phase ac-ac converter modules with four-quadrant bidirectional switches to interface with a three-phase MVAC grid. MF square-wave switching of the line voltage induces a MF voltage on the secondary and tertiary windings. 2-L VSCs connected to the secondary and tertiary windings convert the MF ac voltages to dc voltages. One VSC is used to supply a battery bank, while the other is cascaded with another 2-L VSC connected to a wind turbine, yielding two ac ports and one dc port. Nonetheless, even if only one ac-ac converter module is used per phase, without stacking more modules in series, the switch count is even higher than the converter discussed in the preceding paragraph. As a result, higher complexity and losses can be expected from this converter.

Multi-stage solutions offer flexibility, as several options can be applied to each stage to meet specific criteria of the converter system. Inherent decoupling can also be achieved since each stage works as an independent converter. In general, some common disadvantages of multi-stage converters are their reduced power density, increased losses, higher cost, and increased switch count, Table 1.1; all of which stem from the fact that multi-stage converters are simply multiple converters connected together to achieve the desired input and output power characteristics.

1.3.2 Single-Stage Solutions

In an effort to further increase power density, efficiency and reduce cost, several single-stage converters with HF isolation have been investigated. Converters of this type can process power between one port and another without using more than one conversion stage, usually by multi-

functional control of several power components (e.g., switches and transformers) or by leveraging four-quadrant bidirectional switches, in a similar way as matrix converters do.

One of the key differentiators among single-stage topologies is the transformer power transfer mechanism (Table 1.1). It is evident that the most popular approach to control power transfer across the transformer is phase-shift control. This control technique is based on the DAB converter principle. The square-wave voltages that are imposed on the transformer windings can be a product of the commutation of the switching devices on both sides of the transformer, [27]- [29], [34]- [36], or can be synthesized from a modulating signal [33]. The benefits mentioned in the previous section, regarding DAB converters also apply to single-stage converters that operate under the DAB principle. In the same way, the drawbacks associated with nonlinear control relations and increasing reactive power with higher phase-shift angles are also present in most DAB-based single-stage converters. Moreover, the following additional drawbacks are specifically inherent to some DAB-based single-stage converters:

1. For a given phase-shift angle, the maximum power through the transformer happens when square-wave voltage pulses are applied on both sides of the transformers; in other words, when these square-wave voltages have a duty cycle of 50%. Hence, when the duty cycle is used as a control variable (e.g., to modulate a dc or an ac voltage), the maximum average power that can be transferred through the transformer is effectively reduced, [27]- [29], [34]- [36].
2. In the case of single-phase converters connected to an ac port, the sinusoidal variation of the duty cycle of the square-wave pulses results in LF pulsations appearing in the instantaneous power across the transformer, which increases the decoupling capacitance[5] requirement, [27], [29], [36]. This does not happen in three-phase converters since the ac portion of the LF power signal adds up to zero, [28], [35].

Another strategy to achieve single-stage HF power transfer in isolated converters is to employ resonant elements in the circuit [30], [31]. When these elements are excited at the frequency of resonance, an oscillating current is generated, which flows through the transformer windings,

[5] Also referred to as dc-link capacitance, it acts as a power decoupling element. Hence the term *decoupling capacitance*.

allowing to send power through it. The resonant frequency is often chosen to be equal to the switching frequency, resulting in minimal transformer size. Furthermore, resonant converters can attain soft switching, reducing the commutation losses. Nonetheless, resonant converters are more complex to design and control than pulse-width modulated converters [42] and they tend to suffer from high resonant currents.

Among the ac-dc converters presented in Table 1.1, only one is demonstrated to connect with a three-phase system while attaining single-stage power conversion [28], this allows the converter to be used for high-power applications like EV charging, as it can process more power and it also provides galvanic isolation. The converter employs dual inverter legs, whose outputs are differentially connected on both ends of the windings of three single-phase transformers (one transformer per phase). A center tap in the primary winding of the three transformers allows to connect the converter to a three-phase ac system. To transfer power across the transformer, the converter uses the DAB principle, phase-shifting the triangular carriers of the secondary side with respect to the carriers of the primary side[6]. To generate the ac grid currents, the converter uses a sinusoidal modulating signal that is compared against the carriers to generate the necessary pulse-width modulation (PWM) pulses (i.e., sinusoidal PWM [SPWM]). This facilitates the use of dq-frame current control for the grid power. However, this causes the duty of the square-wave pulses to be different from 50% (see Figure 1.4). Therefore, modulating the pulses that are applied to the windings of the transformers reduces the maximum power that can be transferred across them, as mentioned earlier. The same modulating signal is applied to both the secondary and primary-side carriers to match the resulting PWM pulses imposed on both sides of the transformers, reducing the high reactive currents that would otherwise appear in the transformer windings.

[6] The inverters on each side of the transformer (primary and secondary) have two opposite carriers (i.e., 180° out of phase): one for the inverter legs on the left and another for those on the right (see Figure 1.4).

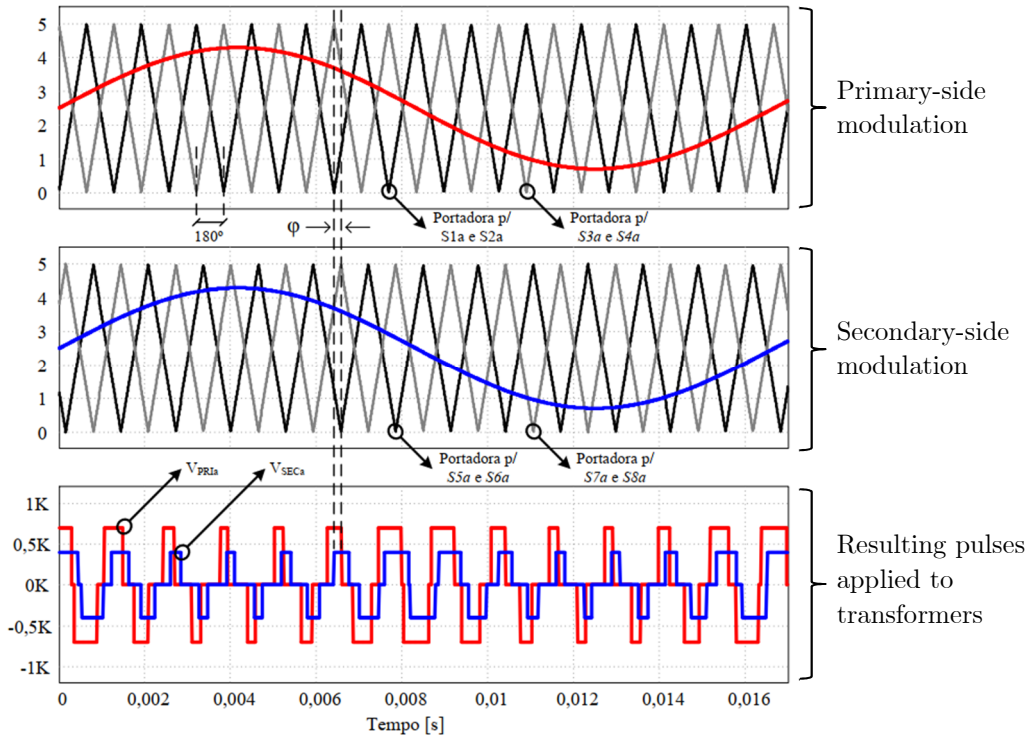

Figure 1.4. Modulation strategy of the dc-ac converter presented in [28] (source: [43]).

It is worth mentioning that a similar concept to the one discussed in the preceding paragraph is used in a single-phase converter [27], Table 1.1. As noted before, the fact that this is a single-phase single-stage converter using SPWM means that a LF pulsating power signal will be present in the transformer windings, increasing the decoupling capacitance requirement, because the capacitor has to process these LF currents, instead of HF currents. The benefit of smaller capacitance requirements is that film capacitors can be used, which are more reliable than their electrolytic counterparts, increasing the converter reliability.

To mitigate these LF pulsations, some strategies can be employed in single-phase single-stage converters. One of these strategies, applied to a converter that combines a DAB and a single-phase VSC [29] (Table 1.1), aims to mitigate the LF pulsations that the dc-side capacitor processes by adding an ac component to the otherwise-constant phase-shift angle. This ac variation of the phase-shift angle is determined by a power decoupling controller that uses two resonant compensators tuned to eliminate the first and second harmonics present in the dc-side currents. As a result, LF pulsations are eliminated from the dc current. The converter, however, requires additional passive elements such as dc and LF ac blocking capacitors in series with the transformer

windings to ensure that only HF components are impressed on the transformer. Moreover, the dc capacitor of the ac-side full bridge still has to be large enough to process LF ac components and achieve decoupling. Another strategy is used in a series-resonant converter that employs half bridges on both sides of the transformer, one of which consists of four-quadrant bidirectional switches, [31] (Table 1.1). It incorporates an active filter on the dc side to eliminate the LF currents, favoring a reduced dc capacitance. In spite of employing half bridges instead of full bridges, the use of four-quadrant bidirectional switches to interface with the ac grid and an active filter, results in a similar switch count as other single-phase single-stage dc-ac converters, [27], [29] (Table 1.1). The issues of LF pulsating power are not present in three-phase single-stage converters, because the ac portion of the instantaneous power adds up to zero in three-phase systems. This statement applies to the converters presented in this thesis.

In regard to isolated multiport converters, a vast array of possibilities exists when it comes to ac and dc ports. For instance, a topology that combines the DAB and two-phase interleaved converter concepts by using a center-tapped transformer and coupled inductors provides multidirectional power to four dc ports, [34] (Table 1.1). It makes use of differential-mode (DM) currents to send power through the transformer employing the DAB principle, and common-mode (CM) currents to send power to the dc ports located at the output of the center taps, by adjusting the duty cycle of the inverter legs. Still, this topology provides no ac ports. By using four-quadrant bidirectional switches in the secondary-side bridge, a similar converter is able to interface two dc ports on the primary side with an ac port on the secondary, [36] (Table 1.1). It does not use center taps in the transformer windings, but rather employs external inductors across the primary-side windings of the transformers, resulting in an interleaved boost converter structure equivalent to the one in [34]. Power control through the HF transformer follows the DAB principle, while power between dc ports is achieved by parallel operation of the boost converter structure in the primary.

In spite of all the possible combinations of dc and ac ports, a closer look at the topologies shown in Table 1.1 shows that no single-stage topologies can attain ac-ac conversion, that is, supporting more than one ac port. Multi-stage converters can achieve this by using cascaded

converters, at the expense of higher component count[7], [32], [33]. Therefore, an insufficiency of HF isolated single-stage multiport converters with ac-ac conversion capability is identified in the literature.

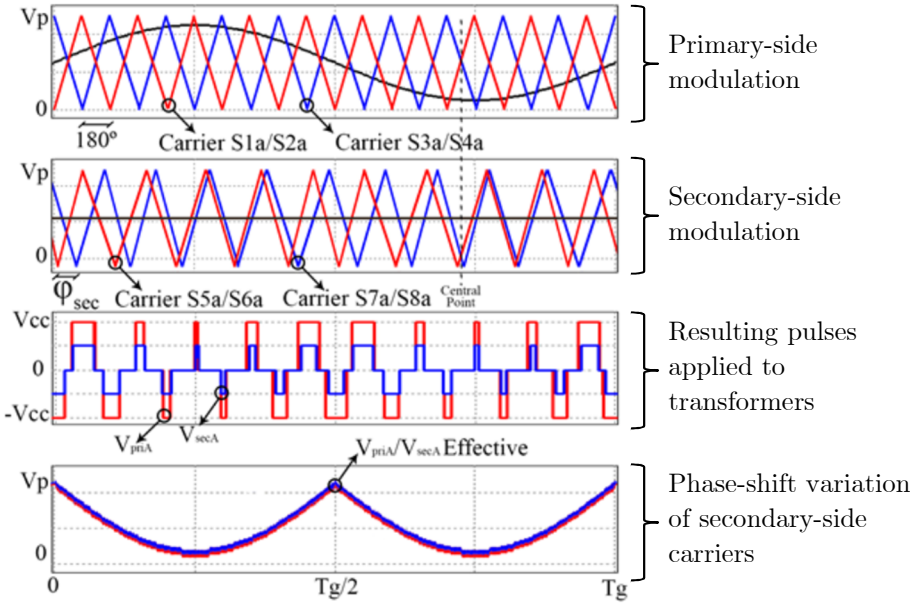

Figure 1.5. Modulation strategy adopted for the multiport converter in [35].

Another aspect to pay attention to, is whether the converters are able to connect to three-phase systems, as this allows them to be used in higher power applications. Among the single-stage multiport converters that accommodate at least one ac port, only two are conceived for three-phase systems. One of these converters combines a three-phase 2-L VSC and a unidirectional three-phase full-bridge converter in a single unit [37]. It boasts the lowest active switch count among the converters presented in Table 1.1, having only six active switches, as required in standard three-phase 2-L VSCs, while offering HF transformer isolation to one of the dc ports. Notwithstanding, the converter only supports bidirectional power flow between the ac port and one of its dc ports, referred to as dc sub-grid (see [37] in Table 1.1). Power exchange with the second dc port, referred to as IBA[8] dc sub-grid, is unidirectional. Furthermore, the voltage of this

[7] An exception is the three-stage SST, which, in spite of being a multi-stage solution, has a low active switch count when using a single-phase DAB, [18], Table 1.1. A discussion on this topology compared to the multiport converter presented in this thesis is given in the next section.

[8] IBA stands for *intermediate bus architecture*. Refer to [37] for details.

port is not actively regulated, but rather kept within a specified range by careful component choice, and additional dc-dc converter stages are necessary downstream. This is a tradeoff for having the lowest switch count and limits the applications of the converter. As a result, only one converter can support bidirectional power between all ports, while offering a three-phase ac connection [35], in addition to the converter presented in this thesis. It is closely related to the DAB-based ac-dc converter discussed previously [28], with two additional dc ports. One is simply the primary-side dc-link and the other has been obtained by adding center taps in the secondary side. This new dc port is intended for a battery, and it is controlled by using a dc level as modulating signal for the secondary-side carriers. Because, unlike the ac-dc version of this converter, different modulating signals are used on both sides of the transformer, the phase-shift between carriers on one side of the transformers is sinusoidally varied (called the secondary phase shift), allowing to closely match the PWM pulses (Figure 1.5) and, in this way, limiting the reactive currents flowing through the windings. The use of this sinusoidally-changing secondary phase shift constrains the center-tap port of the secondary to operate as a dc port, because if the port were modulated using an ac signal, the secondary phase-shift variation would become very cumbersome to determine and implement. Furthermore, as a DAB-based single-stage converter, the drawbacks mentioned before are also true for this topology.

1.4 Thesis Statement

Two converter topologies that provide high-frequency isolation in a single power processing stage are presented in this thesis: an ac-dc bidirectional converter and an ac-ac fully bidirectional multiport converter. An alternative strategy for control of the HF power flow through the transformers is developed, using a completely different approach from the popular DAB-based phase-shift control used in single-stage converters.

The converters offer several advantages over the reviewed topologies:

1. The HF currents are sinusoidal and generated via PWM. Hence, HF power analysis is greatly simplified.
2. Well-established current control techniques can be used for the HF transformer power transfer, such as dq-frame current control, allowing to directly control the HF currents.

3. No reactive currents arise in the transformer windings for increasing HF power transfer because the HF current is controlled to be in phase with the HF voltage at all times.
4. A single carrier is used for controlling all switches, making for a simplified implementation.
5. The dynamics of the HF and LF currents are inherently decoupled thanks to independent CM and DM currents: HF currents for transformer power flow, LF for grid current control.
6. The maximum power that can be sent through the transformers does not depend on the duty-cycle variation that results from the PWM synthesis of ac voltages. In other words, it is independent of the PWM patterns applied to the transformer windings.
7. Low decoupling capacitance is required because there are no LF power pulsations present across the transformer windings. This can enable the use of film capacitors across the dc rails of the grid-side VSCs to increase the reliability of the converter.

Some multi-stage solutions described have a lower switch count than the converters presented in this thesis and can attain soft switching to reduce commutation losses [26], [18]. However, the converters presented here have the following advantages over these solutions:

1. The additional switches contribute to the reliability of the converter: if a switch fails in the single-phase DAB stage of the multi-stage converters, power through the transformer is disrupted, whereas the failure of a switch in either of the presented topologies does not prevent power from being sent through the transformers using the unaffected phases, at a reduced rating.
2. The grid currents are processed in parallel by two inverter legs per phase, reducing the conduction losses of the switches, whereas the 2-L VSCs used in the cited multi-stage converters must process the full ac currents.
3. The ac output filtering requirements are reduced due to the following reasons:
    a. Five-level PWM line voltages are generated at the ac output, unlike the three-level PWM line voltages generated by the 2-L VSCs of the multi-stage converters. This results in increased output current quality.
    b. The frequency of the PWM line voltage is four times the switching frequency, whereas the line voltage generated by the 2-L VSCs of the multi-stage converters is only twice the switching frequency; this also increases output current quality.

c. The leakage inductance of the transformers contributes to the total ac output inductance because the grid currents must flow through the transformer windings.

The converters presented in this thesis share a common magnetic and topological architecture, as well as the principle of operation for the HF power through the transformers. They have been, however, conceptualized for different applications. The topological and control differences, as well as some of the design considerations are better explained by analyzing them separately. Therefore, they are presented in two separate chapters.

The bidirectional ac-dc converter is presented giving an insight into the topology, its operation, and its control scheme (Chapter 2). A simulation model is shown to showcase the parameters of a fine-tuned 10-kW system, followed by the results of a 1.5-kW experimental prototype to validate the concept. Having been originated as an extension of the ac-dc converter, the architecture, operation, and control scheme of the ac-ac multiport converter is presented (Chapter 3). The decoupled bidirectional ac-ac and ac-dc conversion capabilities of the converter are demonstrated using an experimental prototype of 1.3 kW. The key findings are then summarized and a discussion of the multiple possibilities of future work on the presented concepts is given (Chapter 4).

Chapter 2

Bidirectional DC-AC Converter with High-Frequency Isolation

A dc-ac topology is described that applies CM and DM voltages to the windings of three single-phase transformers by means of a multi-frequency modulation strategy. This strategy makes possible to generate the desired HF and LF currents that allow, respectively, to convey power through the transformer and exchange power with the grid. The converter controller uses the dq reference frame for controlling the LF grid current, as well as the transformer HF current, introducing a unique approach for HF power control in single-stage converters. The LF and HF currents are decoupled. The latter is used to control the grid-side converter dc capacitor voltage. A 10-kW simulation model is used to illustrate suitable converter parameters and to demonstrate its dynamic behavior. Finally, a 1.5-kW proof-of-concept prototype is presented, along with results and analysis of its steady-state and dynamic performance.

2.1 Converter System Architecture

The structure of the converter consists of four three-phase 2-L VSCs and three core-type single-phase transformers (one transformer per phase). Two VSCs are differentially connected across the end terminals of the primary windings of the three transformers, and the other two across the end terminals of the secondary windings, Figure 2.1. For reference, VSCs located at the left and right side of the diagram are referred to as VSC 1 and 2, respectively, specifying in which side of the transformers they are located.

The positive and negative rails of the two VSCs on the primary side comprise the dc terminal of the converter (e.g., a battery or a dc bus), while the dc rails of the secondary-side VSCs are connected to a floating capacitor. For simplicity, the turns ratio of the primary and secondary windings is 1:1, but a different ratio could be chosen for voltage step up or step down. The secondary-side winding of the transformers has a center-tap terminal, each connected to a phase of a three-phase ac system. Hence, they comprise the converter's ac terminal.

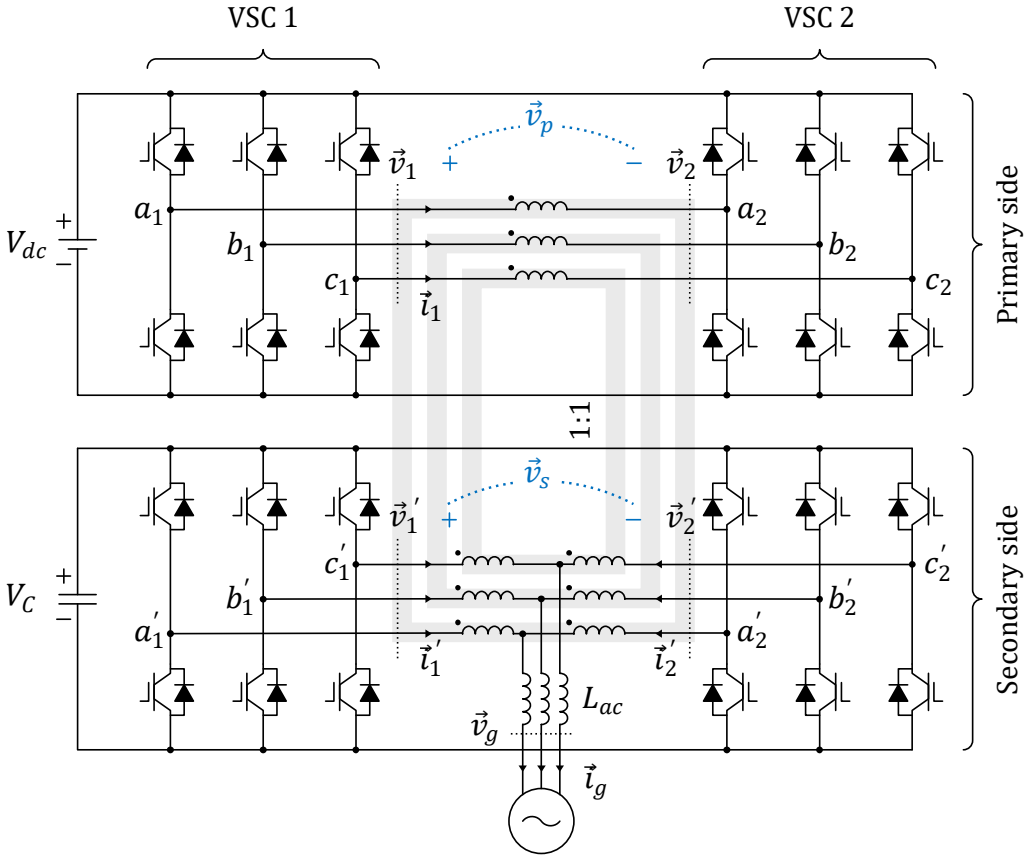

Figure 2.1. Single-stage bidirectional dc-ac converter using three single-phase high frequency isolation transformers.

The converter system is best suited for ac to dc conversion applications where galvanic isolation and/or voltage matching is required, along with bidirectional power flow. It can be used as an EV fast charging station, since it provides a three-phase connection and high-quality input current, enabling high power ratings. Its HF transformer design makes it especially suitable for the on-board charger of an EV. The bidirectional capability of the converter gives the possibility to provide advanced functionalities such as vehicle-to-grid power. The converter can also serve in microgrids where dc and ac voltages coexist, regulating power flow between both domains with

low-volume and low-weight HF isolation ensuring safety and dc-voltage blocking, while providing reactive power support for the ac network.

2.2 Principle of Operation

The differential connection across the transformer windings of the two pairs of VSCs allows to impose CM and DM voltages at the winding terminals. In this manner, in the primary side, a set of three-phase DM voltages is imposed across the windings by synthesizing a three-phase set of HF sinusoidal voltages[9] $\vec{v}_{HF}$ at the output of VSC 1, while VSC 2 synthesizes an equal and opposite set of voltages ($-\vec{v}_{HF}$). Then, the voltage produced by each VSC at the primary side is:

$$\vec{v}_1 = \vec{v}_{HF} \tag{5}$$

$$\vec{v}_2 = -\vec{v}_{HF} \tag{6}$$

The imposed voltage across the primary-side windings is merely the difference between these two voltages:

$$\vec{v}_p = \vec{v}_1 - \vec{v}_2 = 2\vec{v}_{HF} \tag{7}$$

In the secondary side, the same approach to generate a HF sinusoidal DM voltage across the secondary windings of the transformers is employed, with the addition that both VSCs superpose a three-phase set of LF sinusoidal voltages $\vec{v}_{LF}$ of equal polarity at both ends of the windings. This voltage is, therefore, a CM voltage. The resulting voltage synthesized by each VSC of the secondary side can be expressed as

$$\vec{v}'_1 = \vec{v}_{LF} + \vec{v}'_{HF} \tag{8}$$

$$\vec{v}'_2 = \vec{v}_{LF} - \vec{v}'_{HF} \tag{9}$$

Where the superscript ($'$) distinguishes secondary-side quantities that are analogous to quantities of the primary. Like the primary, the resulting voltage across the windings of the secondary side is the difference between these two voltages:

---

[9] Throughout this thesis, space-phasor notation is used to express three-phase balanced time-varying sinusoidal quantities, [44]. Therefore, the space phasor $\vec{x}$ represents the three-phase set of functions $[x_a, x_b, x_c] = [\hat{x}\cos(\omega t + \theta), \hat{x}\cos(\omega t + \theta - 2\pi/3), \hat{x}\cos(\omega t + \theta - 4\pi/3)]$, where $\hat{x}$, ω and θ are the amplitude, angular frequency and initial phase angle of the sinusoidal functions.

$$\vec{v}_s = \vec{v}_1' - \vec{v}_2' = 2\vec{v}_{HF}' \tag{10}$$

Note that the LF voltages $\vec{v}_{LF}$ superposed by both VSCs of the secondary are not present across the secondary-side windings. From (7) and (10) we can arrive at the conclusion that no LF voltages are present on either side of the transformers and, as a result, only HF flux is induced, allowing to reduce the size and weight of the transformer cores.

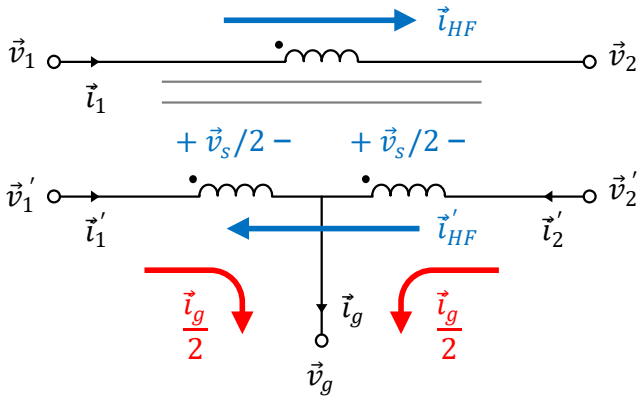

Figure 2.2. Per-phase representation of transformer terminal voltages and currents of the dc-ac converter.

The preceding analysis concerns the voltages present across the windings. To calculate the voltage present at the center-tap terminals, consider the per-phase circuit of the transformer windings, Figure 2.2. Neglecting the voltage drop across the ac output inductance L_{ac} and defining a fictitious midpoint voltage reference of $V_C/2$ for the secondary-side voltages, Kirchhoff's voltage law (KVL) can be applied starting from the center-tap terminal of the secondary windings to obtain the following voltage-loop equations:

$$\vec{v}_g = -(\vec{v}_s/2) + \vec{v}_1' \tag{11}$$

$$\vec{v}_g = (\vec{v}_s/2) + \vec{v}_2' \tag{12}$$

Adding (11) and (12) and substituting (8) and (9) yields

$$\vec{v}_g = \frac{\vec{v}_1' + \vec{v}_2'}{2} = \vec{v}_{LF} \tag{13}$$

This means that the only voltage present at the center-tap terminals consists of a grid-compatible three-phase LF voltage. None of the HF voltages used to transfer power through the transformer are seen by the grid.

PWM is used to generate the voltages of each VSC. The modulating signals $\vec{m}_1$ and $\vec{m}_2$ are used to generate the voltage output of both VSCs in the primary side, and they comprise only two opposing HF sinusoidal signals, Figure 2.3(a). For the secondary-side VSCs, the modulating signals $\vec{m}'_1$ and $\vec{m}'_2$ are used, Figure 2.3(c). Unlike the primary-side modulating signals, the two signals have also a LF component present. These multi-frequency modulating signals can be obtained by simply adding a LF signal $\vec{m}$ to the corresponding HF signals $\vec{m}'_{1HF}$ and $\vec{m}'_{2HF}$, Figure 2.3(b). The LF signal $\vec{m}$ is then responsible for the synthesis of the CM voltages and the HF signals $\vec{m}'_{1HF}$ and $\vec{m}'_{2HF}$ for the synthesis of the DM voltages. This modulation scheme requires a single triangular carrier for all inverter legs of the VSCs, streamlining its implementation.

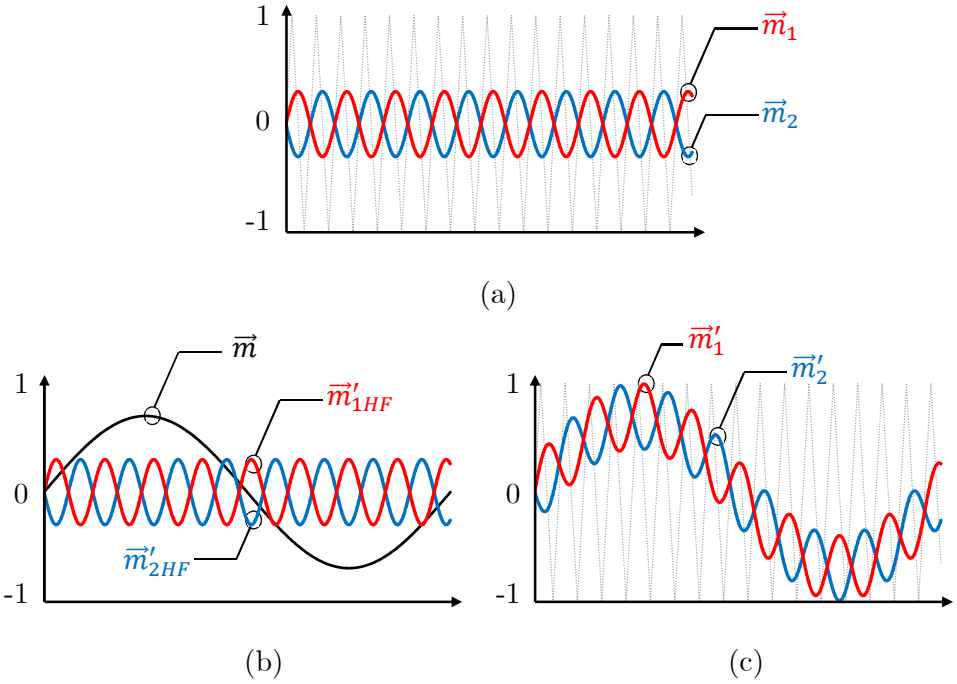

Figure 2.3. Modulation strategy of dc-ac converter. (a) Primary-side modulating signals. (b) Components of secondary-side modulating signals [low frequency ($\vec{m}$) and high frequency ($\vec{m}'_{1HF}$, $\vec{m}'_{2HF}$)]. (c) Resulting secondary-side modulating signals $\vec{m}'_1$ and $\vec{m}'_2$.

The DM voltages $\vec{v}_p$ and $\vec{v}_s$ applied across the transformer windings generate a HF current that flows from one VSC to the other, as a DM current, Figure 2.2. In the primary side, the differential-mode HF current $\vec{\imath}_{HF}$ is the only component flowing through the windings. Thus

$$\vec{\imath}_{HF} = \vec{\imath}_1 \tag{14}$$

Where $\vec{\imath}_1$ is the output current of VSC 1. In the secondary side, the common-mode LF grid current $\vec{\imath}_g$ flows together with the differential-mode HF current $\vec{\imath}'_{HF}$. These current components can be obtained from the measured output currents $\vec{\imath}'_1$ and $\vec{\imath}'_2$ of both VSCs as follows:

$$\vec{\imath}_g = \vec{\imath}'_1 + \vec{\imath}'_2 \tag{15}$$

$$\vec{\imath}'_{HF} = \frac{\vec{\imath}'_2 - \vec{\imath}'_1}{2} \tag{16}$$

The calculation of these currents is essential for the control scheme presented in the next section.

2.3 Control Scheme

The goals of the controller are to regulate the active and reactive power exchange with the ac grid, while keeping the secondary-side capacitor voltage V_C at the desired level. In order to achieve these goals, power taken from or sent to the capacitor by the grid should be balanced by power received from or sent to the dc terminal through the HF transformers. These objectives are fulfilled by the three main control loops detailed in the following subsections, Figure 2.4.

2.3.1 Grid Current Controller

The grid current controller supervises the power exchanged with the grid by the converter. It controls both active and reactive power, and it is implemented using dq-frame current control. Because this control scheme is well understood and widely implemented in grid-connected converters, it is explained from a high-level perspective. The contents of the grid current controller block (Figure 2.4) and details of its design can be consulted in [44, pp. 204-244].

The reference currents i^*_{gdq}, obtained from the power relations in dq-frame [44, p. 219], are compared with the actual grid currents $\vec{\imath}_g$ converted to dq quantities[10] i_{gdq}, and the error is passed to the internal proportional-integral (PI) regulators, to ensure accurate reference tracking. The grid currents are obtained according to (15). For a given controller bandwidth $1/\tau_{i1}$, the proportional k_{p1} and integral ki_1 gains of these regulators can be calculated as

[10] Quantities expressed with the notation x_{dq} represent the d and q-axis components $[x_d, x_q]$.

$$k_{p1} = L_{ac}/\tau_{i1} \tag{17}$$

$$k_{i1} = \frac{R_{ac} + R_{eq}/8}{\tau_{i1}} \tag{18}$$

Where the numerator of (18) is the total resistance in the path of $\vec{\imath}_g$, Figure 2.2. R_{ac} is the equivalent output resistance from the center-tap terminals to the grid and R_{eq} is the transformer equivalent series resistance.

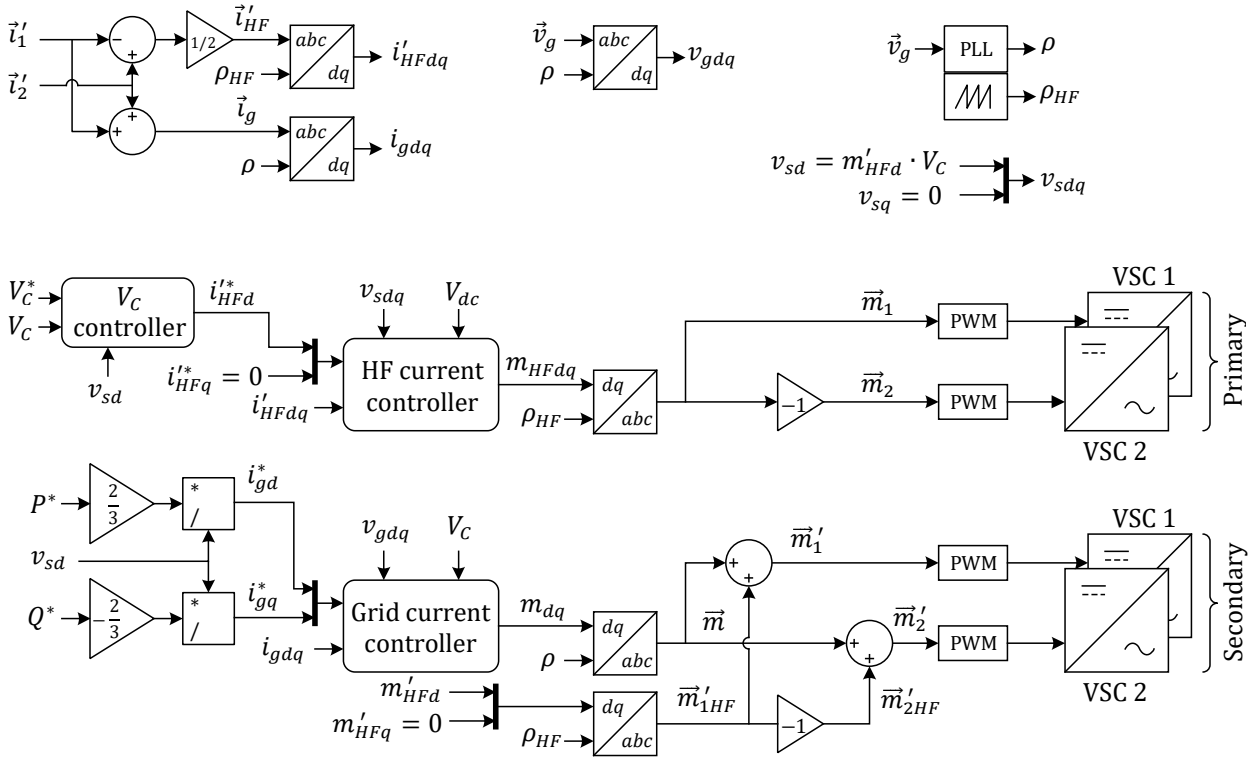

Figure 2.4. Controller for the single-stage bidirectional dc-ac converter.

The grid controller uses the dq-axis components of the grid voltage v_{gdq} and V_C as feedforward signals to improve its dynamic performance. A phase-locked-loop (PLL) provides the angle ρ for the reference frame transformations using the three-phase grid voltage measurement $\vec{v}_g$. After applying the corresponding dq to abc transformation, the output of this controller is the LF signal $\vec{m}$ shown in Figure 2.3(b).

2.3.2 High-Frequency Current Controller

The HF current controller regulates the HF power transfer through the transformers. To do this, it uses the DM voltages applied to the windings on both sides of the transformers to generate a current that flows through the transformer impedance. Consider the transformer equivalent circuit, Figure 2.5. Assuming that the impedance of the magnetizing branch (grayed out in Figure 2.5) is very large compared to the leakage inductance, the magnetizing current can be neglected and, therefore, the primary and secondary HF currents can be considered approximately equal $\vec{\imath}_{HF} \approx \vec{\imath}'_{HF}$, resulting in a circuit of two voltage sources, $\vec{v}_p$ and $\vec{v}_s$, connected through the transformer equivalent series resistance R_{eq} and the leakage inductance L_{eq}.

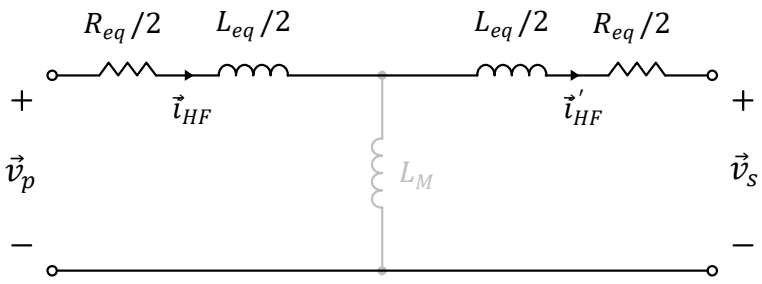

Figure 2.5. Transformer equivalent circuit for the HF currents. L_M is the transformer magnetizing inductance.

$\vec{v}_s$ is kept fixed at a constant amplitude by the secondary-side inverter[11], while the magnitude and phase of $\vec{v}_p$ is controlled by the primary-side inverter to drive the desired HF three-phase sinusoidal current $\vec{\imath}'_{HF}$, in a similar way as a grid-connected VSC, where the grid can be modeled as a fixed voltage source with a series impedance, through which the VSC drives a current according to the desired command. Because of this similarity, the HF current controller can be designed in a similar way as the grid current controller, using a standard control technique like dq-frame current control, [44, pp. 204-244].

First, the secondary-side HF current is calculated via (16) using the measured currents $\vec{\imath}'_1$ and $\vec{\imath}'_2$. This current is then transformed to the HF dq-frame quantities i'_{HFdq} and compared to the

[11] Another possibility could be to keep $\vec{v}_p$ constant while varying $\vec{v}_s$, however, $\vec{v}_s$ has been chosen to be constant because we are interested in the power received at the secondary side, where the floating capacitor is connected. In this manner, any losses from the primary to the secondary side do not have to be accounted for by the capacitor voltage controller.

reference currents i'^{*}_{HFdq}. The resulting error signal is passed to the internal PI regulators of the control block. By analyzing the transformer equivalent circuit, Figure 2.5, and considering the similarity of the circuit with that of a grid-tied VSC, the PI compensator gains of this controller can be derived as

$$k_{p2} = L_{eq}/\tau_{i2} \tag{19}$$

$$k_{i2} = R_{eq}/\tau_{i2} \tag{20}$$

In these equations, $1/\tau_{i2}$ is the bandwidth of the HF current controller. The derivation of the PI compensator gains is, therefore, straightforward, as it is only necessary to measure the transformers equivalent leakage inductance L_{eq} and resistance R_{eq} between the primary and secondary, using, for example, an LCR meter.

In this converter, the leakage inductance provides controllability of the HF current and, additionally, helps to filter the switch-mode reactive currents that arise due to PWM pattern differences across the transformer. Thus, a relatively loose coupling between primary and secondary windings (e.g., 0.95 as in transformers with windings on separate limbs) is preferred over a very tight coupling (e.g., 0.99 as in layered windings on the same limb). Alternatively, a transformer design with tightly coupled windings could be used, but small external filter inductors would be needed at the output of the inverter legs of the VSCs that constitute the converter.

To decouple the dynamics of the capacitor voltage from the response of the HF current controller, V_{dc} and v_{sdq} are passed as feedforward signals, Figure 2.4. v_{sdq} represents the dq-axis voltage components of secondary-side windings $\vec{v}_s$, obtained from

$$v_{sdq} = \left[v_{sd}, v_{sq}\right] = [m'_{HFd} \cdot V_C, 0] \tag{21}$$

Where m'_{HFd} is the percentage (from 0 to 1) that represents how much of the modulation depth of the secondary-side VSCs is exclusively set aside for the HF component of the modulating signal. Referring back to the modulation scheme, Figure 2.3, we know that the secondary-side inverters are modulated with two superposed signals of different frequencies. These two signals, $\vec{m}$ and $\vec{m}'_{1HF}$ (or $\vec{m}'_{2HF}$ for VSC 2), must add up to a maximum value of 1, to avoid overmodulation, meaning that the dc voltage V_C of these two VSCs is shared by both the LF and HF output voltages.

Considering that the HF reference frame is aligned with v_{sd}, the amplitude $\hat{v}_s$ of the secondary-side winding voltage is determined by m'_{HFd} for a given capacitor voltage V_C, according to (21). Observing the transformer equivalent circuit, Figure 2.5, it is evident that a higher amplitude of the DM voltage $\vec{v}_s$ will result in smaller HF currents for a given transformer power transfer. However, increasing $\vec{v}_s$ means that a higher capacitor voltage V_C is required, because, as stated previously, the capacitor voltage is used by the secondary-side VSCs to synthesize both the LF and HF components. The dc voltages needed to generate the LF (i.e., CM) component depend mainly on the grid voltage and the voltage drop across the output impedance (in the same way as a standard grid-tied VSC), whereas the additional dc voltage required to generate the HF (i.e., DM) component depends on the chosen amplitude of $\vec{v}_s$. As a result, in this converter, a tradeoff has to be made between higher dc capacitor voltage and higher HF winding currents. However, this is not the case for the primary-side dc voltage V_{dc} because it only has to generate HF voltages. Thus, the voltage requirement of the primary-side dc source is considerably lower than V_C.

Note that the reference angle of the HF reference frame transformations ρ_{HF} is generated by a wrapping integrator[12], Figure 2.4, whose frequency f_{HF} determines the frequency of the DM signals. As a rule, f_{HF} should not be higher than one decade of the switching frequency f_{sw} for the controller to remain stable.

The output of the HF current controller, once the appropriate dq to abc transformations have been applied, is the primary-side inverter HF modulating signal $\vec{m}_1$, from which the opposite signal $\vec{m}_2$ is obtained (both shown in Figure 2.3(a)).

The total HF power measured at the secondary-side windings of all three transformers can be calculated using the power equation in dq-frame as:

$$P_{HF} = (3/2) v_{sd} i'_{HFd} \tag{22}$$

Therefore, controlling i'_{HFd} allows to set the HF transformer power transfer. Equation (22) shows that, unlike DAB-based single-stage converters, average HF transformer power transfer is

[12] A *wrapping integrator* serves as a clock whose value increases with time until it reaches an upper boundary (e.g., 2π), resetting to its lower boundary (e.g., 0), in order to avoid the overflow of variables.

completely independent of the ac grid modulation depth[13]. Moreover, the time-domain instantaneous power per phase at the secondary windings is expressed as:

$$P_{HF,1\phi}(t) = \frac{\hat{\imath}'_{HF}\hat{v}_s}{2}[cos(2\omega_{HF}t + \theta_{HF}) + \cos\theta_{HF}] \tag{23}$$

Where $\hat{\imath}'_{HF}$ and θ_{HF} are the amplitude of the secondary-side HF currents and the phase angle between $\hat{\imath}'_{HF}$ and $\vec{v}_s$ (maintained at zero by the controller), and $\omega_{HF} = 2\pi f_{HF}$ is the frequency of the DM signals in radians per second. Equation (23) shows that, for a single phase, the power across the transformer has an ac (i.e., pulsating) component at twice the HF of the DM signals. It follows that a single-phase version of the dc-ac converter presented here would have a lower decoupling capacitance requirement compared to the single-phase single-stage DAB-based converters reviewed earlier (Table 1.1) because the capacitor would not have to deal with LF pulsations[14].

2.3.3 Capacitor Voltage Controller

The capacitor voltage controller is the outermost control loop. It regulates the voltage of the floating capacitor in the secondary side. To achieve this, the controller sets the d-axis reference value i'^{*}_{HFd} of the inner HF current controller (Figure 2.4) to ensure that the instantaneous power flowing out of the capacitor $-P_C$ to the grid is matched by the instantaneous HF power P_{HF} received from the primary through the transformers (and vice versa), fulfilling the following power balance condition

$$P_{HF} - P_C = 0 \tag{24}$$

Where

$$P_C = V_C I_C \tag{25}$$

[13] This can be corroborated by evaluating the effect of the ac grid modulation depth M in equation (5) of [27] and in equations (6) and (7) of [29]. Also, see Figure 4 of [28].

[14] The presence of the duty cycle d in the instantaneous power equation (4) of [27] is an example of this. Also, in [29] they use phase-shift modulation to eliminate the LF pulsations in the dc-side capacitor, but the LF component (of two times the line frequency) must still be processed by the ac-side capacitor.

In (25), the capacitor current I_C is defined as flowing into the capacitor. Substituting (22) and (25) in (24) and clearing for i'_{HFd} yields

$$i'_{HFd} = \frac{2}{3v_{sd}} V_C I_C \tag{26}$$

The dynamic equation of the capacitor current is

$$I_C = C\frac{dV_C}{dt} \tag{27}$$

Therefore, the transfer function that relates the capacitor current with the capacitor voltage is

$$G(s) = \frac{V_C}{I_C} = \frac{1}{sC} \tag{28}$$

Using (26) and (28) and considering that the inner HF current controller is much faster than the capacitor voltage controller, ensuring that $i'^{*}_{HFd} \approx i'_{HFd}$, a controller using a PI compensator can be designed to keep the capacitor voltage at the desired level, Figure 2.6.

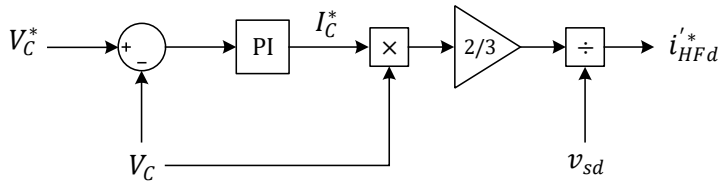

Figure 2.6. Detail of the capacitor voltage controller block.

The PI compensator used for this controller is of the form

$$K(s) = k_{p3}\left(1 + \frac{\omega_i}{10s}\right) \tag{29}$$

From where $\omega_i = 2\pi/t_{i3}$ is the controller bandwidth in rad/s (t_{i3} is the controller bandwidth in Hz) and k_{p3} can be calculated using the capacitance C of the floating capacitor in the secondary side:

$$k_{p3} = \left|\frac{1}{\left(1 + \frac{1}{j10}\right)(j\omega_i C)}\right| \tag{30}$$

2.4 Simulation

The dc-ac converter and its controller were validated initially using simulations in PLECS. To showcase the main characteristics of the converter, the simulated model employs fine-tuned parameters for a 10-kW grid-tied system. The simulation case is first introduced, then the results are presented and discussed.

2.4.1 Model

The parameters of the simulated converter are summarized in Table 2.1. Note that the primary-side dc voltage V_{dc} is lower than the capacitor voltage V_C, since the primary-side VSCs only need to generate a HF voltage high enough to overcome the transformers' impedance voltage drop and the secondary-side HF voltage, which is defined by $\hat{v}_s = m'_{HFd} \cdot V_C = 200\,V$. As will be demonstrated in the results discussion, choosing the HF component modulation depth to be 40% of the dc capacitor voltage (i.e., $m'_{HFd} = 0.4$) allows to match the transformers' winding rms currents with the grid rms currents.

The frequency of the transformer HF DM voltage is chosen as $f_{HF} = 2\,kHz$ here. A higher frequency could be chosen if the switching frequency is increased, allowing to further reduce the size and weight of the transformers. However, increasing f_{HF} also means that the voltage drop across the impedance of the transformer leakage inductance $j\omega_{HF}L_{eq}$ will increase, resulting in a higher primary-side dc voltage requirement to overcome this additional voltage drop. Hence, a smaller leakage inductance will be preferred at higher values of f_{HF}.

The value of the capacitor is highly influenced by the bandwidth of the capacitor voltage controller $1/\tau_{i3}$ and the acceptable voltage tolerance during transients. Higher bandwidths allow to choose smaller capacitance values for a given voltage deviation tolerance. It must also be noted that, although f_{HF} is over 33 times higher than the grid frequency f_{ac}, the HF current controller bandwidth $1/\tau_{i2}$ does not have to be 33 times higher than the grid current controller bandwidth $1/\tau_{i1}$ because the HF current controller operates on quantities that have been transformed to a synchronous reference frame (i.e., it works with dc quantities). Thus, the choice of $1/\tau_{i2}$ merely depends on the desired transient response of the HF current controller and not on f_{HF}. Here, the

HF current controller has been empirically chosen to be over 8 times faster than the grid current controller, with satisfactory results. Furthermore, an advantage of using dq-frame to control the HF currents is that, increasing f_{HF} to reduce the size and weight of the transformers does not mean that the bandwidth of the HF current controller has to be proportionally increased, as this controller operates with dc quantities in the HF dq-axis reference frame.

Table 2.1. Simulation parameters

Parameter	Symbol	Value
System rated power	P_{rated}	$10\ kW$
Primary-side dc voltage	V_{dc}	$270\ V$
Secondary-side dc cap. voltage	V_C	$500\ V$
Grid phase rms voltage	$v_{g,RMS}$	$120\ V$
AC output inductance	L_{ac}	$0.5\ mH$
AC output resistance	R_{ac}	$1\ m\Omega$
Grid frequency	f_{ac}	60 Hz
Secondary-side dc capacitance	C	$50\ \mu F$
HF modulation depth	m'_{HFd}	0.4
HF voltage signal frequency	f_{HF}	$2\ kHz$
Switching frequency	f_{sw}	$30\ kHz$
Transformer equivalent resistance	R_{eq}	$0.2\ \Omega$
Transformer leakage inductance	L_{eq}	$274\ \mu H$
Grid current controller bandwidth	$1/\tau_{i1}$	2 kHz
HF current controller bandwidth	$1/\tau_{i2}$	16.7 kHz
Cap. voltage controller bandwidth	$1/\tau_{i3}$	2 kHz

2.4.2 Results

The simulation case starts with the converter operating in steady state, sending 10 kW to the ac grid. Then, at $t = 26.7\ ms$ the power command is reversed, drawing 10 kW from the ac grid to the dc source, Figure 2.7. The power reversal happens in less than a third of a line cycle. The duration of this transient is mainly due to the bandwidth of the grid current controller $1/\tau_{i1}$.

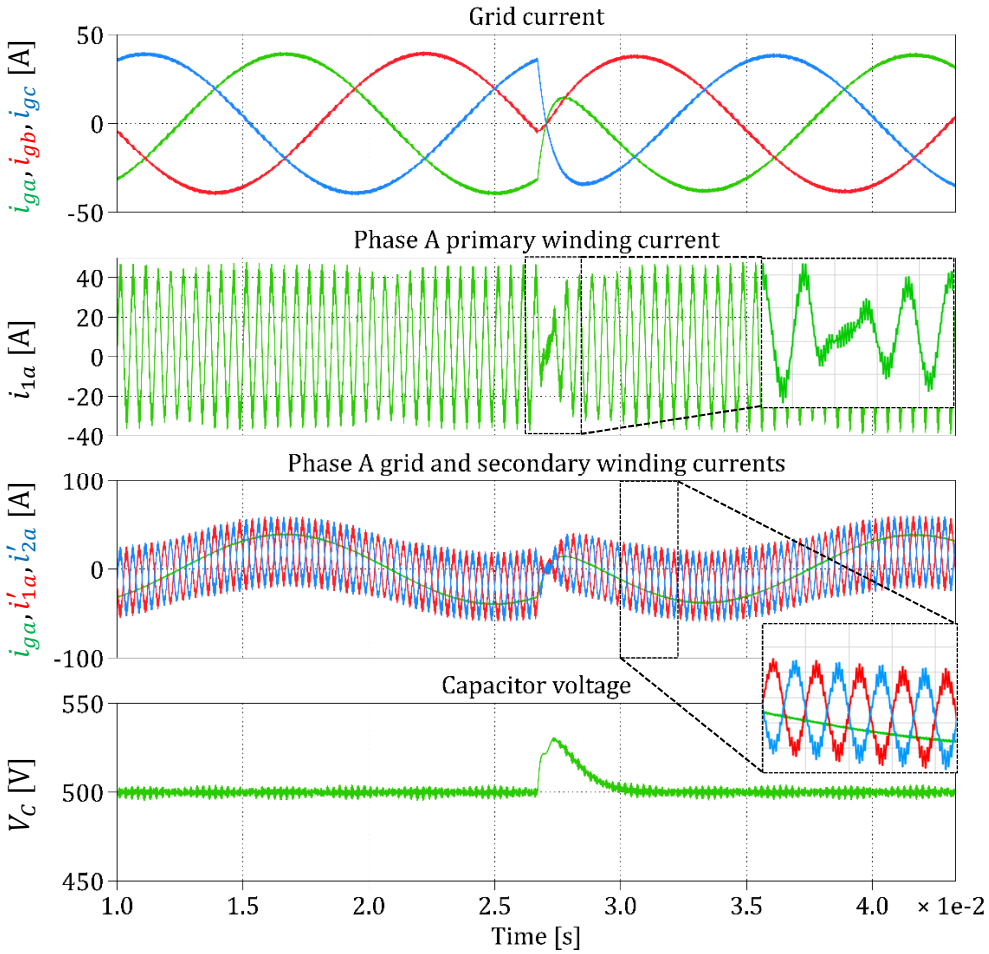

Figure 2.7. Simulated system response under a power reversal.

Throughout the simulation, the current to (and from) the grid is close to 27.7 A rms with a THD of less than 2%. It contains no current components at f_{HF}, since these currents only exist in the DM. The waveform of the primary winding currents only consists of a high-frequency DM component, in agreement with (14), while the secondary winding currents contain both a low-frequency CM component and a high-frequency DM component in each phase (see close up in the third plot of Figure 2.7). The waveforms of the secondary winding current show opposite HF components and equal LF components (see i'_{1a} and i'_{2a} in Figure 2.7). This is due to the direction of the measured winding currents $\vec{\imath}'_1$ and $\vec{\imath}'_2$, Figure 2.1, and confirms that the HF currents flow between VSCs, while the LF currents flow in parallel from each VSC to the grid (as shown in Figure 2.2).

Before the power is reversed, the rms current flowing through the windings is 25.2 A for the primary and 27.7 A for each of the secondary windings (similar values are measured after the power change). Hence, the currents flowing through each phase of the grid and the currents passing through each winding have similar rms values, which means that the windings can be rated for the same power level as the output wiring. As mentioned earlier, this has been achieved by choosing a value of m'_{HFd} that results in HF currents that are sufficiently low to match the rms currents of the grid. However, the peak of the secondary winding currents is expected to be about 35% larger than the grid current amplitude, even if the switching ripple is ignored, due to the sum of the amplitudes of $\vec{\imath}'_{HF}$ (33 A) and $\vec{\imath}'_g/2$ (19.5 A), which are the currents that flow through the secondary windings, Figure 2.2. The switching ripple increases the peak currents depending on the switching frequency f_{sw} and the leakage inductance L_{eq}. In this case it results in a peak current about 50% larger (59 A) than the peak grid current (40 A).

The capacitor voltage is successfully kept constant at 500 V. After the power reversal command, the capacitor voltage increases to 530 V (only 6% above the reference), since power is now coming from the grid, before being brought back to 500 V by the controller. The voltage transient lasts less than 5 ms. To avoid capacitor voltage buildup, the HF current command $\vec{\imath}'^{*}_{HFd}$ is reversed by the external voltage controller, and the inner HF current controller ensures that the actual HF currents $\vec{\imath}'_{HF}$ (and consequently $\vec{\imath}_{HF}$) are reversed. This can be seen in the primary winding current i_{1a} right after the transient, Figure 2.7. Therefore, the power coming from the grid is immediately transferred at 2 kHz through the transformers and rectified to feed the dc source in the primary side.

The results show that the converter can respond to abrupt changes in power demand in less than a third of a grid cycle, while maintaining the capacitor voltage at the desired value using a small decoupling capacitance. This allows to use a film capacitor, resulting in increased reliability and power density compared to converters with electrolytic capacitors.

2.5 Experimental Prototype

A 1.5-kW proof-of-concept experimental prototype was used to validate the converter and the controller operation, and to confirm its dynamic and steady-state operation. The parameters of

the experimental prototype were dictated by the available components in the laboratory and not optimized for its power level. Hence, the primary goal of the testing was to demonstrate the concept of achieving LF grid current control using a HF transformer.

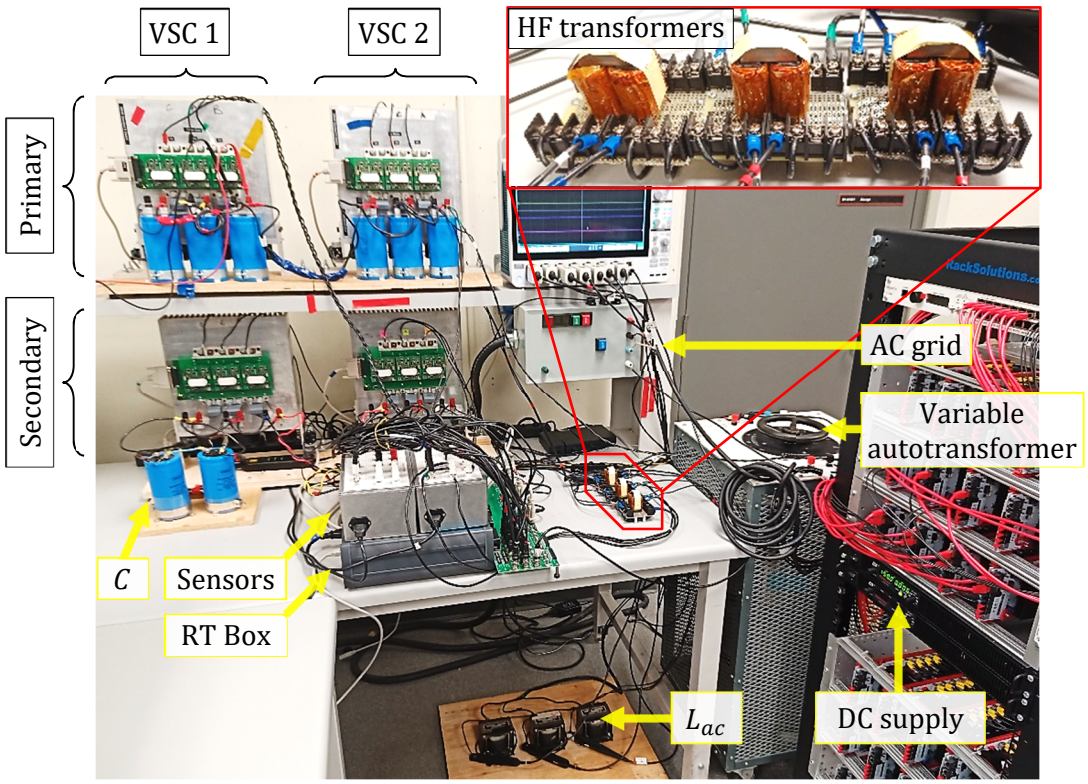

Figure 2.8. Experimental prototype, testing setup and close-up of HF transformers of dc to ac converter.

Four custom-built 2-L VSCs employing Semikron SKiM306GD12E4 IGBT power modules were controlled using a PLECS RT Box, Figure 2.8. A computer running a PLECS model linked to the RT Box in real time was used to send the desired commands to the converter. The primary-side dc rail voltage was set to 300 V by two 1.5-kW Sorensen XG 300-5 dc supplies connected in parallel. Two 450-V 2-mF electrolytic capacitors in series were connected to the dc rails of the secondary-side VSCs, providing a decoupling capacitance of 1 mF. Three single-phase C-core transformers with the primary and secondary windings wound on separate limbs were employed as the HF transformers. The center-tap terminals of the secondary windings were connected to the low-voltage side of a variable autotransformer connected to a three-phase ac grid. The variable autotransformer was used to adjust the voltage of the grid to 50% of its 120-V phase voltage nominal value (i.e., to 60 V phase voltage). The currents and voltages required for control purposes

were measured using LEM HAS 50-S and LEM LV 25-400 sensors, respectively, contained in custom-made sensor boxes, and their signals sent to the analog inputs of the RT Box. A summary of the parameters of the experimental system is given below.

Table 2.2. Parameters of the experimental dc to ac converter prototype.

Parameter	Symbol	Value
System rated power	P_{rated}	1.5 kW
Primary-side dc voltage	V_{dc}	300 V
Secondary-side dc cap. voltage	V_C	300 V
Grid phase rms voltage	$v_{g,RMS}$	60 V
AC output inductance	L_{ac}	2.5 mH
AC output resistance	R_{ac}	1 $m\Omega$
Grid frequency	f_{ac}	60 Hz
Secondary-side dc capacitance	C	1 mF
HF modulation depth	m'_{HFd}	0.4
HF voltage signal frequency	f_{HF}	2 kHz
Switching frequency	f_{sw}	40 kHz
Transformer equivalent resistance	R_{eq}	0.8 Ω
Transformer leakage inductance	L_{eq}	1.1 mH
Grid current controller bandwidth	$1/\tau_{i1}$	2 kHz
HF current controller bandwidth	$1/\tau_{i2}$	16.7 kHz
Cap. voltage controller bandwidth	$1/\tau_{i3}$	20 Hz

2.5.1 Experimental Test

The experimental test (Figure 2.9) starts with the converter sending half the rated power to the grid (750 W). Then, the power command is increased to the rated power (1.5 kW). The reactive power is kept at 0 VAR during the whole test. Throughout the test, the controller monitors the primary and secondary dc voltages, and the currents through the windings to ensure that the safety thresholds[15] are not exceeded at any time. If this happens, the controller opens all IGBTs, disconnecting the converter from the grid and avoiding damage to components.

To reach steady-state conditions, first the capacitor voltage is gradually built by changing the reference voltage V_C^* in steps. Once 300 V are reached the grid is connected, with the variable

[15] These thresholds were set at 320 V for the primary-side dc link, 600 V for the dc capacitor in the secondary side and 40 A peak for the winding currents.

transformer already adjusted to 50% of its nominal voltage. The power is first increased from 0 to 750 W and then the final power setpoint of 1.5 kW is applied. An analog signal output from the RT Box synchronized with the scope trigger was simultaneously changed from low to high to capture the power command transient, Figure 2.9.

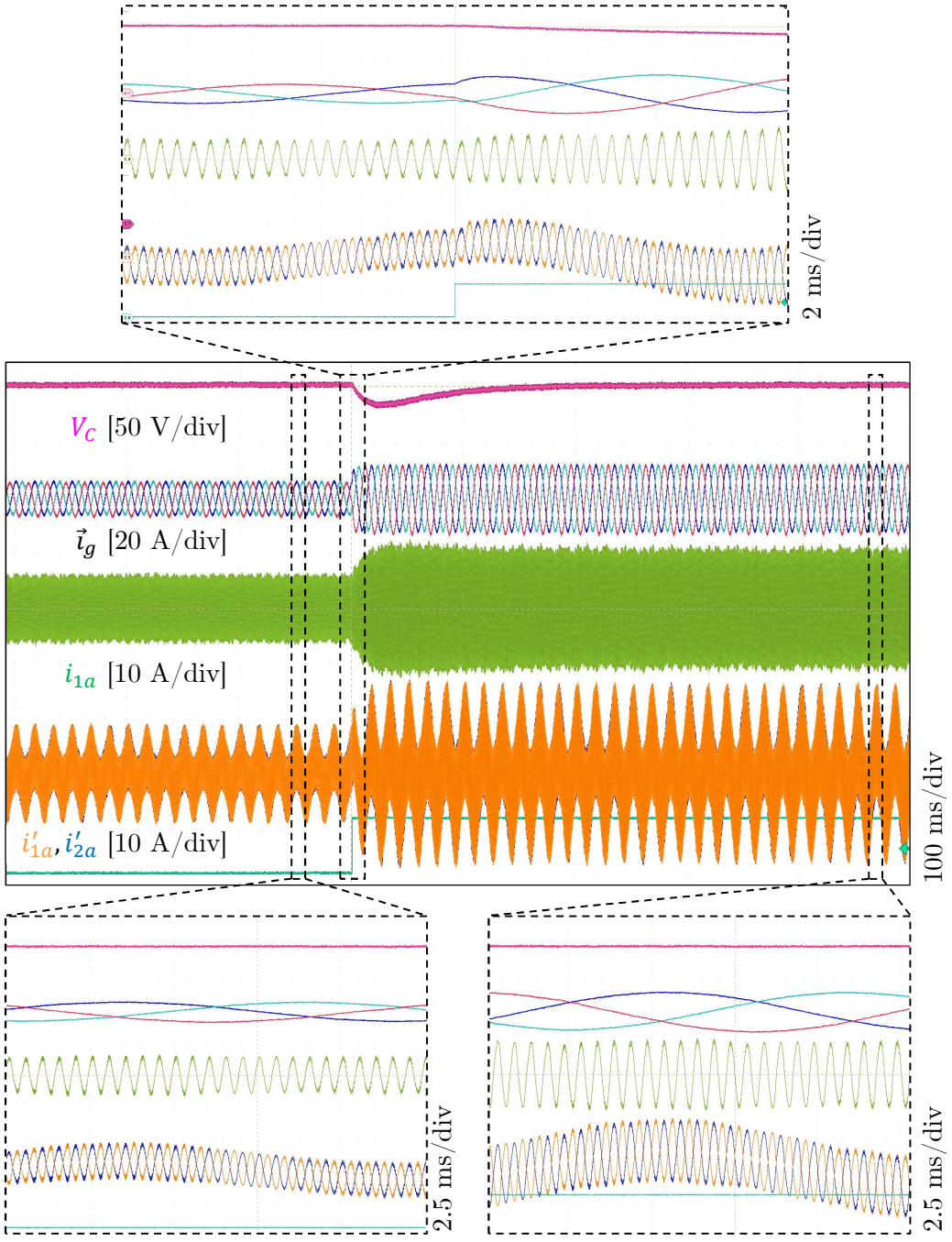

Figure 2.9. Key waveforms of the experimental prototype response under a power increase command from half to rated power.

2.5.2 Results

The key waveforms of the experimental test, Figure 2.9, are in good agreement with the simulated waveforms, Figure 2.7. The grid current waveforms show that the converter is able to reach the commanded rated power output within two line cycles.

The primary-side winding current i_{1a} is exclusively a 2-kHz sinusoidal waveform, while the currents measured through both secondary windings, i'_{1a} and i'_{2a}, contain a 2-kHz component on top of a 60-Hz component. The measurement direction of the current probes is the same as shown in Figure 2.1; hence, the 2-kHz component is flowing between VSCs and the grid-frequency component flows from the two secondary-side VSCs to the grid. The grid currents are free from any 2-kHz component, Figure 2.9, achieving a THD of 3.4% at half the rated power and 1.9% at rated power, because this HF component only exists as a DM current.

Similar to the simulation case, the rms currents flowing through the transformer windings are closely matched with the rms value of the grid currents. At rated power, the primary winding currents are equal to 7.2 A and the secondary winding currents are equal to 7.8 A, whereas the grid currents are equal to 8.4 A. The correlation of rms currents also holds at half power, being equal to 3.8 A for the primary windings and 4.2 A for the secondary windings and the grid. At full power, the peak currents through the secondary windings (16.5 A) are 32% larger with respect to the peak grid currents (12.5 A), and 42% larger at half power (9.1 A peak through the windings and 6.4 A peak to the grid). The peak currents must be considered when selecting the switching devices.

The controller is able to maintain the capacitor voltage at 300 V throughout the test, deviating by only 21 V (7%) below the reference when the power change is commanded, and settling after 250 ms, as the capacitor voltage controller has been tuned for a slower response than in the simulation to reduce noise feedback to the minimum.

A close examination of the transient reveals that, as soon as the power to the grid increases, the capacitor voltage starts to dip. Then, in order to keep the voltage constant, the controller reacts by increasing the HF current component, sending more power to the capacitor from the primary-side dc source and bringing its voltage back to the reference value. The HF current

component is not reversed in the experimental test because the direction of the grid power is maintained.

The test shows that the converter operates as expected from the simulations, following the desired power command to the grid, and maintaining the decoupling capacitor at the desired voltage level, while generating a high-quality low-THD grid current.

2.6 Summary

Dual inverters (i.e., VSCs) allow to impose DM and CM voltages on the transformer windings. These voltages produce currents in two different domains (i.e., CM and DM) and, thus, are decoupled. A multi-frequency modulation scheme superposes high-frequency DM and low-frequency CM signals to generate the secondary-side voltages. Only high-frequency DM modulating signals are used to synthesize the primary voltages. The DM currents are HF ac sinusoids that flow between VSCs to induce HF flux in the transformer cores and convey power through them. The CM currents are LF ac sinusoids that flow in parallel from the dual inverters to the ac grid.

Synchronous (i.e., dq) reference frames operating at the corresponding frequency (transformer or grid frequency) are leveraged to allow independent control of ac grid power and HF transformer power. Implementation is therefore streamlined, as the derivation of the transformer power controllers is similar to the well-known grid current controller in dq frame. The similarity becomes evident when analyzing the transformer equivalent circuit. A PI controller ensures that the dc capacitor in the secondary side is kept constant, by giving the appropriate current reference to the HF controller.

The bidirectional capability of a 10-kW converter is demonstrated in a simulation environment. A full power reversal showed that the decoupling capacitor voltage can be kept within 6% of the reference, even when a small capacitance of 50 μF is used. Results from a 1.5-kW prototype subjected to a step change in power from half to rated power are in good agreement with the simulated waveforms. Even though DM and CM currents coexist in the transformer windings, the rms currents flowing through them are shown to be similar to the grid currents. Hence, the windings can be rated for the same power level as the output wiring. The grid currents are free

from the HF component used for the transformer power transfer and have a high quality, demonstrating the suitability of the converter for grid-connected applications.

Chapter 3

Multiport AC-AC Converter with High-Frequency Isolation

The operation of a multiport converter that has an ac-ac power conversion capability is presented. The converter uses DM and CM signals to achieve decoupled control of two dc ports and two three-phase ac ports. The multi-frequency modulation strategy used in the dc to ac converter is extended to generate the necessary HF and LF voltages of the multiport converter. A dq reference frame is used to control the transformer low and HF current components. A unique aspect of the converter control is its capability to have ac voltages of differing frequencies on its two ac ports. The asynchronous operation of its two ac ports is validated using a 1.3-kW experimental system prototype circuit. The system dynamic response is demonstrated by subjecting the converter to a full power reversal. A discussion of the benefits of this multiport converter is given, using the results obtained from the experimental testing.

3.1 Converter System Architecture

The multiport converter presented consists of four three-phase 2-L VSCs. As with the dc to ac converter presented in the previous chapter, two of these VSCs are differentially connected across the primary-side windings of three HF single-phase transformers, and the other two are differentially connected across the secondary windings, Figure 3.1. For reference, the three inverter legs on the left side of the schematic are named VSC 1, and on the right side, VSC 2, specifying on which side of the transformers they are. The two dc ports of the converter are formed by the

positive and negative dc rails of the VSCs. Each dc port is, therefore, isolated from each other. Two three-phase ac ports are made available by providing center tap terminals on the windings of both sides of the transformers. The two ac ports are also isolated with respect to each other.

The differentially connected VSCs can impose both a CM and DM voltage across the transformer windings. These two voltage components are leveraged to allow decoupled control of the ac port voltages (CM voltage) and the HF transformer voltage (DM voltage).

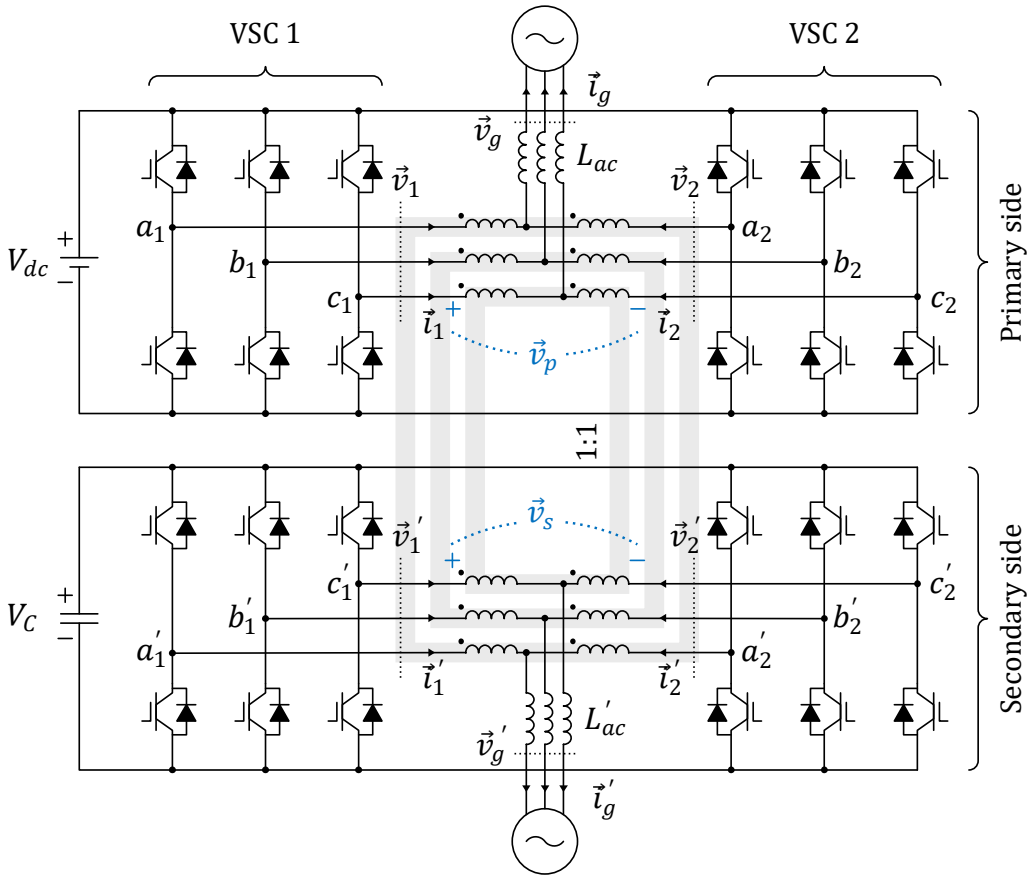

Figure 3.1. Multiport converter using three single-phase high-frequency isolation transformers (cores shown in gray).

This multiport converter can find applications such as:

1. An ac-ac converter for asynchronous grids (e.g., to interconnect 50 and 60-Hz grids), if capacitors are used in both dc ports, providing isolation between both grids and reactive power support.
2. An SST serving as an interconnection point for hybrid ac-dc grids, allowing to control power flow among two dc ports (e.g., photovoltaic generators, fuel cells, dc buses) and two ac ports (e.g., ac grids, diesel generators, motor loads).

3. A wind energy conversion system (WECS) by employing one ac port as a VFD and the other to connect to an ac grid; in this application, a battery can be connected to the generator-side dc port to provide energy storage and a capacitor at the grid-side dc port, providing reactive power support, and voltage step-up choosing the appropriate turns ratio.

3.2 Principle of Operation

To understand the principle of operation of the converter, consider first the transformer primary-side windings, Figure 3.1. VSC 1 can synthesize a three-phase set of HF sinusoidal voltages $\vec{v}_{HF}$, while VSC 2 synthesizes an equal and opposite set of voltages (i.e., $-\vec{v}_{HF}$). This results in a three-phase DM voltage across the transformer primary windings with an amplitude of $2\vec{v}_{HF}$. Both VSCs can also produce a low-frequency CM voltage across the transformer primary windings, $\vec{v}_{LF}$, which results in LF voltages at the windings' center tap terminals. The resulting LF currents do not produce flux in the transformer cores. Referring to Figure 3.1, the output voltages of each VSC at the primary can be expressed as

$$\vec{v}_1 = \vec{v}_{LF} + \vec{v}_{HF} \tag{31}$$

$$\vec{v}_2 = \vec{v}_{LF} - \vec{v}_{HF} \tag{32}$$

Hence, the voltage across the primary windings is

$$\vec{v}_p = \vec{v}_1 - \vec{v}_2 = 2\vec{v}_{HF} \tag{33}$$

Following the same analysis for the secondary side, yields

$$\vec{v}_s = \vec{v}_1' - \vec{v}_2' = 2\vec{v}_{HF}' \tag{34}$$

As in the previous chapter, the superscript ($'$) refers to secondary-side quantities analogous to those of the primary side. Equations (33) and (34) are equivalent to equations (7) and (10) of the dc to ac converter, showing that the transformers only see HF voltages across their windings on both sides, which allows to reduce their size and weight. None of the LF components are applied to the transformers because only the HF voltages are of DM nature and appear as a voltage potential across the transformer windings.

The LF voltage at the primary-side center-tap terminals can be found from (31) and (32) as

$$(\vec{v}_1 + \vec{v}_2)/2 = \vec{v}_{LF} \tag{35}$$

This equation shows that no HF voltages appear at the center taps. A similar relation applies to the secondary side:

$$(\vec{v}'_1 + \vec{v}'_2)/2 = \vec{v}'_{LF} \tag{36}$$

The PWM modulation scheme used for the dc to ac converter is extended here to allow for an additional ac port. Unlike the dc to ac converter, the primary-side modulating signals $\vec{m}_1$ and $\vec{m}_2$ that generate the voltage output of both VSCs not only consist of two opposing HF sinusoidal signals; they also have a superposed LF sinusoidal signal with the frequency of the primary-side ac port. The same strategy is used for the secondary-side modulating signals $\vec{m}'_1$ and $\vec{m}'_2$, having two opposing HF sinusoidal signals and a superposed LF sinusoidal signal, with the difference that this LF component is synchronized with frequency of the secondary-side ac port.

These multi-frequency modulating signals are obtained by the addition of a LF signal $\vec{m}$ with the corresponding HF signals $\vec{m}_{1HF}$ and $\vec{m}_{2HF}$, Figure 3.2(a). The LF signal $\vec{m}$ is responsible for the synthesis of the CM voltages and the HF signals $\vec{m}_{1HF}$ and $\vec{m}_{2HF}$ for the synthesis of the DM voltages of the primary side. The same procedure is followed to obtain the secondary-side modulating signals. Again, this modulation scheme only employs one triangular carrier for all VSCs, simplifying its implementation.

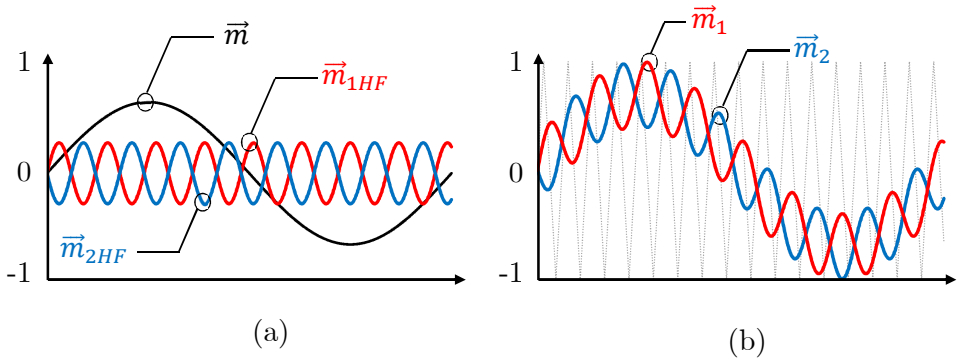

Figure 3.2. Modulation strategy of multiport converter. (a) Common ($\vec{m}$) and differential-mode ($\vec{m}_{1HF}$ and $\vec{m}_{2HF}$) components of the modulating signals of the primary-side VSCs ($\vec{m}_1$ and $\vec{m}_2$). (b) Modulating signals of VSC 1 ($\vec{m}_1$) and VSC 2 ($\vec{m}_2$) of the primary. A similar strategy is followed for the secondary-side VSCs.

To transfer power through the transformers, the same principle of operation as the dc to ac converter is used: the HF voltage applied to the secondary windings $\vec{v}_s$ is kept at a constant

amplitude, while the magnitude and phase of $\vec{v}_p$ is controlled to drive the desired current across the transformer leakage inductance L_{eq} and equivalent resistance R_{eq} (refer to the transformer equivalent circuit, Figure 2.5). This allows to choose a standard current control technique to regulate the sinusoidal HF currents through the transformer. dq-frame current control is also employed for the multiport converter.

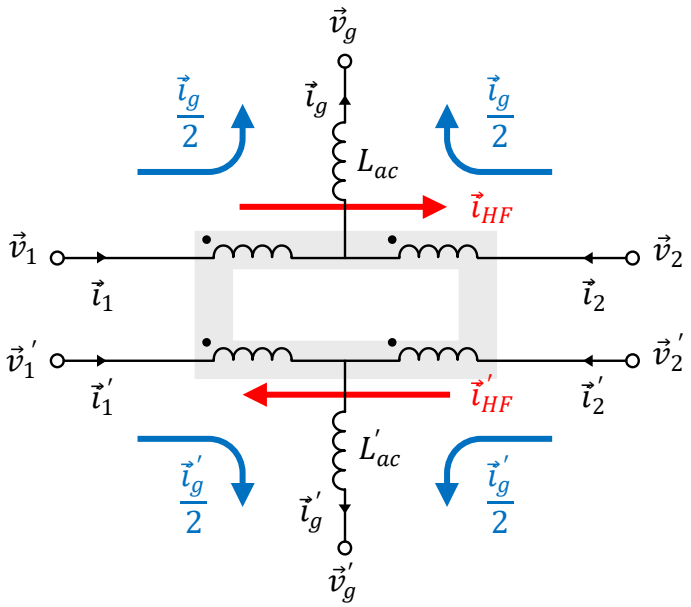

Figure 3.3. Per-phase representation of transformer terminal voltages and currents of the multiport converter.

The voltages applied to the windings result in CM and DM currents sharing the same conductors but following different paths, Figure 3.3. The grid currents ($\vec{\imath}_g$ and $\vec{\imath}_g'$) are of CM nature, and flow in parallel from both VSCs to their respective ac ports; hence, each VSC generates the full grid voltage ($\vec{v}_g$ and $\vec{v}_g'$), but processes only half of the grid current and, therefore, half of the grid power. These currents can be obtained from the output currents of the VSCs using the following relations

$$\vec{\imath}_g = \vec{\imath}_1 + \vec{\imath}_2 \tag{37}$$

$$\vec{\imath}_g' = \vec{\imath}_1' + \vec{\imath}_2' \tag{38}$$

On the other hand, the HF transformer currents ($\vec{\imath}_{HF}$ and $\vec{\imath}_{HF}'$) are of DM nature. They only flow through the windings between VSCs; therefore, each VSC processes the full HF current, but they only generate half of the DM voltage that is impressed across the windings. Hence, each VSC

only processes half of the transformer power. The following equations allow to calculate the primary and secondary-side HF currents using the measured output currents of the VSCs

$$\vec{\imath}_{HF} = \frac{\vec{\imath}_2 - \vec{\imath}_1}{2} \tag{39}$$

$$\vec{\imath}'_{HF} = \frac{\vec{\imath}'_2 - \vec{\imath}'_1}{2} \tag{40}$$

3.3 Control Scheme

The multiport converter presented here is versatile and can be implemented in multiple ways. To showcase the ac-ac conversion capabilities of the converter and the inherently decoupled control of all its ports, in this thesis, the multiport converter is implemented by interfacing an ac grid operating at 60 Hz on the secondary-side ac port with a load operating at 50 Hz connected to the primary-side ac port. The primary-side dc port is connected to a dc supply and the dc port at the secondary is connected to a capacitor. The capacitor maintains the dc voltage required for the operation of the secondary-side VSCs and serves to showcase the dynamic response of the control scheme, since average power exchange with the capacitor must be equal to zero and therefore it should be tightly regulated.

The goals of the controller are to regulate power exchange with the 60-Hz ac grid and the 50-Hz ac load, and to keep the secondary-side capacitor voltage V_C at the desired level by balancing the HF power flow through the transformers with the instantaneous power flow of the capacitor. The power flow of the primary-side dc port meets any power imbalance between the ac ports as it is controlled by a fixed-voltage dc supply (this would be the case for a dc grid connected to this port, for example). The four main control loops explained in the following subsections ensure that these objectives are met, Figure 3.4.

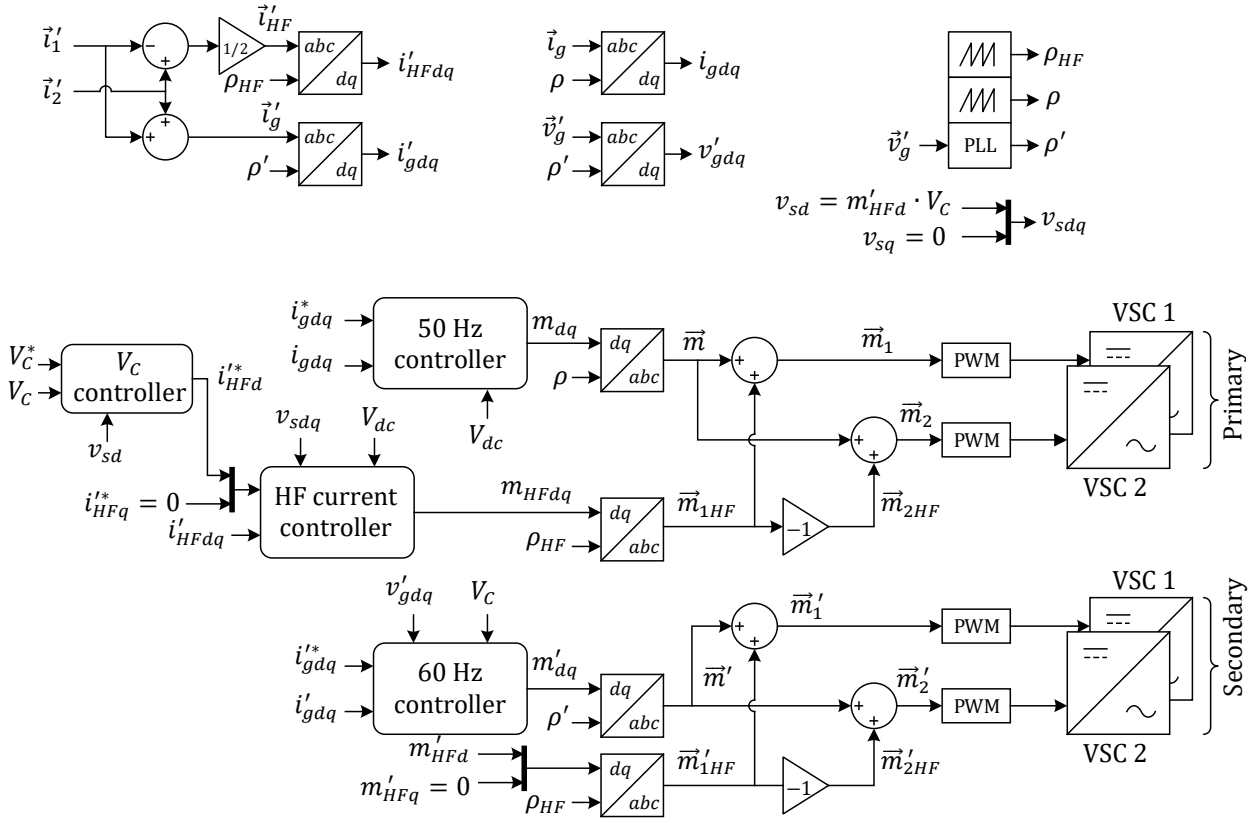

Figure 3.4. Controller for the single-stage multiport converter.

3.3.1 Grid Current Controllers

This converter has two grid current controllers labeled 50 Hz controller and 60 Hz controller, Figure 3.4. Each of these blocks controls the power exchanged with the ac ports under their supervision. The blocks are implemented using dq-frame current control[16].

The 60 Hz controller regulates active and reactive power exchanged with the ac grid and has the same design and equations as the grid current controller of the dc to ac converter. It is reproduced here with the particular notation that applies to the multiport converter. The PI compensators inside the 60 Hz controller block ensure accurate reference tracking by keeping the difference between the reference currents i'^{*}_{gdq} and the actual grid currents i'_{gdq} close to zero. The reference currents i'^{*}_{gdq} are computed from the power relations in dq-frame [44, p. 219], and the grid currents in dq-frame i'_{gdq} are obtained by applying a rotating reference frame transformation

[16] dq-frame current control is well known and, hence, out of the scope of this thesis. Refer to [44, pp. 204-244] for details on the design and contents of such controllers.

to the three-phase grid currents $\vec{\imath}_g'$, which are calculated entering the secondary-side VSCs output currents into (38). The proportional k_{p1} and integral ki_1 gains of these PI compensators can be calculated as

$$k_{p1} = L'_{ac}/\tau_{i1} \tag{41}$$

$$k_{i1} = \frac{R'_{ac} + R_{eq}/8}{\tau_{i1}} \tag{42}$$

R'_{ac} and $1/\tau_{i1}$ are the equivalent output resistance from the center-tap terminals to the grid and the bandwidth of the controller, respectively. R_{eq} is the transformer equivalent series resistance. Only $1/8$ of the transformer equivalent resistance appears in (42) because the grid current $\vec{\imath}_g'$ flows in parallel through two windings, each of which contributes to $1/4$ of R_{eq} (see the path of $\vec{\imath}_g'$ in Figure 3.3).

The 60 Hz controller uses the dq-axis components of the grid voltage v_{gdq} and V_C as feedforward signals to improve its dynamic performance. A PLL provides the angle ρ' for the reference frame transformations using the three-phase grid voltage measurement $\vec{v}_g$. After applying the corresponding dq to abc transformation, the output of this controller is the LF signal $\vec{m}'$.

The 50 Hz controller sets how much active power is sent to the ac load[17]. The design is very similar to the 60 Hz controller, with a few particularities, as its corresponding port is connected to an ac load and not an ac grid:

- First, it does not employ a PLL to generate the angle ρ of the reference-frame transformations; a wrapping integrator with a frequency of 50 Hz is used instead.
- Also, the ac-port output currents $\vec{\imath}_g$ are directly measured at the output of the primary-side center-tap terminals of the transformers; they are not obtained using (37), as this would mean using six current measurements: the three output currents of VSC1 ($\vec{\imath}_1$) and the three output currents of VSC2 ($\vec{\imath}_2$). A similar strategy of only measuring the output ac currents $\vec{\imath}_g'$ in order to reduce the number of current sensors cannot be used with the secondary-side grid currents, because all six VSC output

[17] If a 50-Hz grid were connected to the primary-side ac port, bidirectional power would also be possible, as well as reactive power control. An RL load was employed here, as no 50-Hz ac grid was available at the laboratory.

currents (three of $\vec{\imath}_1'$ and three of $\vec{\imath}_2'$) are needed to calculate the secondary-side HF current component $\vec{\imath}_{HF}'$ (using (40)).

- The final difference of the 50 Hz controller with respect to the 60 Hz controller lies in the feedforward signals: as the voltage is set by the resistive-inductive (RL) load impedance and the power output, no ac voltage feedforward is needed, only the primary-side dc voltage V_{dc} is needed (see Figure 3.4).

The proportional k_{p2} and integral ki_2 gains of the internal PI compensators of this block can be calculated as

$$k_{p2} = L_{ac}/\tau_{i2} \tag{43}$$

$$k_{i2} = \frac{R_{ac} + R_{eq}/8}{\tau_{i2}} \tag{44}$$

The overall output of this controller is the LF signal $\vec{m}$ (shown in Figure 3.2).

3.3.2 High-Frequency Current Controller

The HF controller is exactly the same as the one presented for the dc to ac converter. For brevity, only a summary and equations that, due to notation, differ from those of Chapter 2 are presented here.

In the same way as grid-connected VSCs, the equivalent circuit of the transformers for the high-frequency DM currents (Figure 2.5) consists of a fixed ac source ($\vec{v}_s$) connected to a variable ac source ($\vec{v}_p$) controlled to produce the desired current ($\vec{\imath}_{HF}'$) through the impedance between them ($R_{eq} + j\omega_{HF}L_{eq}$, where ω_{HF} is the frequency in radians of the high-frequency DM currents).

The controller takes the measured currents at the output of the secondary-side VSCs ($\vec{\imath}_1'$ and $\vec{\imath}_2'$) and, using (40) and transforming the result to dq-frame quantities, obtains the dq-axis components of the HF currents in the secondary side i_{HFdq}'. These components are compared to the reference currents $i_{HFdq}'^*$ and the error is minimized by the internal PI compensators of the control block. The compensator gains of this can be obtained from

$$k_{p3} = L_{eq}/\tau_{i3} \tag{45}$$

$$k_{i3} = R_{eq}/\tau_{i3} \tag{46}$$

In these equations, $1/\tau_{i3}$ is the bandwidth of the HF current controller.

The transformer leakage inductance L_{eq} is used to control these HF sinusoidal DM currents. Increasing the leakage inductance by choosing a relatively loose coupling between primary and secondary windings (e.g., 0.95, as in transformers with windings on separate limbs) increases controllability and filters the switch-mode reactive currents arising from PWM pattern differences across the transformer. However, its value should consider the voltage drop that results from the impedance of L_{eq} at the frequency of the DM currents (see the impedance between $\vec{v}_p$ and $\vec{v}_s$ in the transformer equivalent circuit, Figure 2.5), as a higher voltage drop across this impedance will translate in higher amplitude for the HF voltage component, forcing the dc ports to have a higher voltage.

The HF transformer power flow for all three single-phase transformers is governed by (22). The HF voltage imposed at the secondary windings v_{sdq} and the capacitor voltage V_C are sent as feedforward signals to improve the dynamic response of the controller. The d-axis of the HF reference frame is aligned with $\vec{v}_s$. Therefore, as per (21), the amplitude of the voltage imposed on the secondary-side windings $\vec{v}_s$ is equal to the product of the capacitor voltage V_C and the portion (m'_{HFd}) of this capacitor voltage that is reserved to synthesize the HF voltages. A higher amplitude of $\vec{v}_s$ will result in smaller HF currents for a given transformer power transfer (see (22) and Figure 2.5) at the expense of higher dc voltage requirements (V_{dc}, V_C), because the dc voltages are used by the VSCs on both sides of the transformers to synthesize both the LF (i.e., CM) and HF (i.e., DM) components[18]. As a result, a tradeoff has to be made between lower dc-port voltages and smaller HF winding currents.

A wrapping integrator with frequency f_{HF} generates the HF reference frame transformations ρ_{HF}. The frequency of the wrapping integrator determines the frequency of the HF currents. f_{HF} should not be higher than one decade of the switching frequency f_{sw} for the controller to remain stable.

[18] Recall that, different from the dc to ac converter, which only synthesizes both the LF and HF components in the secondary-side VSCs, the multiport converter has these two components generated by the VSCs on both sides of the transformer.

After applying the necessary dq to abc frame transformations, the HF current controller outputs the primary-side inverter HF modulating signal $\vec{m}_1$, from which the opposite signal $\vec{m}_2$ is obtained (shown in Figure 3.2(a)).

3.3.3 Capacitor Voltage Controller

Since the secondary-side dc port is connected to a capacitor, an external voltage control loop sets the current reference of the HF controller i'^{*}_{HFd} to maintain the voltage of the secondary dc port V_C at the desired level (Figure 3.4). The structure and derivation of the controller is the same as for the dc to ac converter of Chapter 2. The following is a brief summary of the key points of this controller.

The controller balances the instantaneous power flowing out of the capacitor $-P_C$ with the instantaneous HF power P_{HF} received from the primary through the transformers (this also applies in reverse power flow), fulfilling the power balance condition in (24). It uses a PI compensator with the structure shown in Figure 2.6. The form of the compensator is as follows:

$$K(s) = k_{p4}\left(1 + \frac{\omega_i}{10s}\right) \tag{47}$$

From where $\omega_i = 2\pi/t_{i4}$ is the controller bandwidth in rad/s (t_{i4} is the controller bandwidth in Hz). The gain k_{p4} can be obtained using the capacitance C in the following expression:

$$k_{p4} = \left| \frac{1}{\left(1 + \frac{1}{j10}\right)(j\omega_i C)} \right| \tag{48}$$

Equations (47) and (48) are the same as (29) and (30) used in the derivation of the capacitor voltage controller of the dc to ac converter. The only difference is the nomenclature of the compensator gain k_{p4}, as the multiport converter has an additional control loop.

3.4 Experimental Prototype

The operation and dynamic response of the converter system and its controller are demonstrated using an experimental proof-of-concept system, Figure 3.5. The same three single-phase transformers and custom-built 2-L VSCs used for the dc to ac converter are employed for the multiport converter. However, different from the ac to dc converter, the primary-side windings

have a center tap terminal to provide an additional ac port, where an RL load is connected. The load consists of three single-phase 5 mH reactors, one per phase, connected in series with a resistive load bank, adjusted to provide a 7.3 Ω resistance. To minimize the number of analog inputs used for the controller and taking into consideration that the RL load is balanced, only two phase currents (i_{ga} and i_{gb}) are measured for control purposes. The third phase current is calculated via

$$i_{gc} = -(i_{ga} + i_{gb}) \tag{49}$$

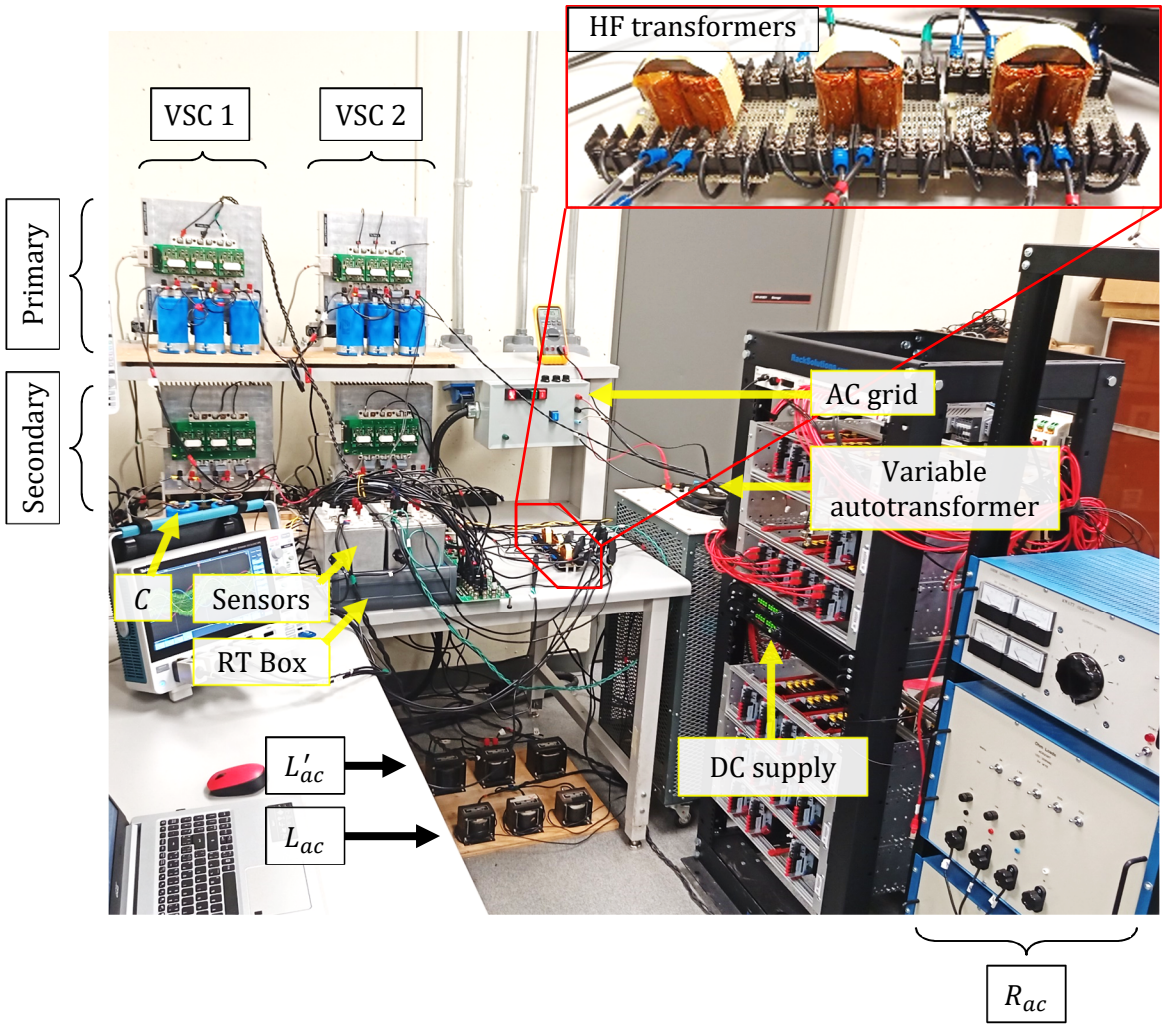

Figure 3.5. Experimental prototype and testing equipment of multiport converter.

A PLECS RT Box acts as the controller, receiving the analog current and voltage measurements and generating the PWM pulses of the four VSCs. Power flow commands are set using a computer linked to the RT Box in real time. Two parallel-connected 1.5-kW Sorensen XG

300-5 dc supplies are set to provide 300 V for the primary-side dc port. The 1-mF decoupling capacitance at the secondary is kept at 300 V.

The secondary-side center tap of the transformers is connected to the ac grid via three single-phase 2.5-mH filter inductors (one per phase) and a variable autotransformer. The autotransformer is used to scale down the grid voltage to 50% (i.e., to 60 V phase voltage) of its nominal value. The specifications of the experimental system are listed below.

Table 3.1. Parameters of the experimental multiport converter prototype.

Parameter	Symbol	Value
Primary ac port three-phase load	L_{ac}, R_{ac}	$5\ mH, 7.3\ \Omega$
Primary ac port frequency	f_{ac}	$50\ Hz$
Primary dc port voltage	V_{dc}	$300\ V$
Secondary ac port phase voltage	$v'_{g,RMS}$	$60\ V$
Secondary ac port output inductance	L'_{ac}	$2.5\ mH$
Secondary ac port frequency	f'_{ac}	60 Hz
Secondary dc port voltage	V_C	$300\ V$
Secondary dc port capacitance	C	$1\ mF$
HF modulation depth	m'_{HFd}	0.4
HF voltage signal frequency	f_{HF}	$2\ kHz$
Switching frequency	f_{sw}	$40\ kHz$
Transformer equivalent resistance	R_{eq}	$0.8\ \Omega$
Transformer leakage inductance per winding	$L_{eq}/4$	$0.3\ mH$
60 Hz controller bandwidth	$1/\tau_{i1}$	2 kHz
50 Hz controller bandwidth	$1/\tau_{i2}$	2 kHz
HF current controller bandwidth	$1/\tau_{i3}$	16.7 kHz
Cap. voltage controller bandwidth	$1/\tau_{i4}$	20 Hz

3.4.1 Experimental Test

The objective of the experimental testing was to demonstrate bidirectional ac-ac power conversion capabilities of the multiport converter and how power balance among all four ports is achieved by the converter. The test also demonstrates that the converter can operate two asynchronous ac ports and that the dynamics of the ports are decoupled, meaning that power fluctuations in one port do not impact the behavior of other ports.

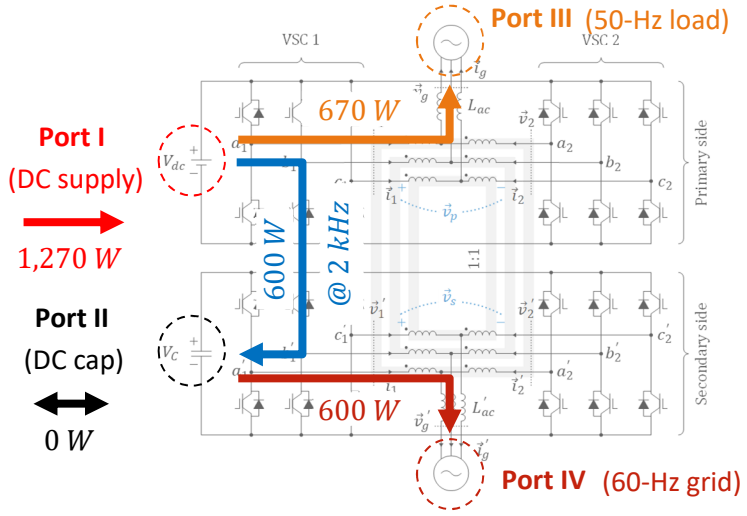

(a)

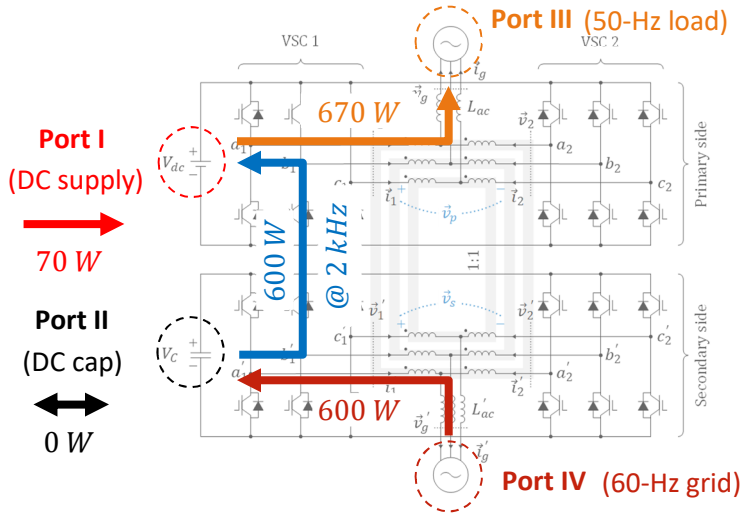

(b)

Figure 3.6. Ideal port power flow during experimental test. (a) Before power reversal. (b) After power reversal.

The test consists of two parts:

- In the starting condition, the converter is in steady state, with the primary-side RL load drawing 670 W from the converter, operating at a frequency of 50 Hz. Simultaneously, on the secondary-side ac port, the converter is sending 600 W to the grid, which operates at a frequency of 60 Hz. The resulting 1.27 kW that the converter sends to both ac ports are provided by the dc supply connected to the primary-side dc port. Therefore, the 600 W that are being sent to the ac grid must be transferred at HF through the transformers

and, to keep zero average power stored in the capacitor (and, hence, a constant capacitor voltage), those 600 W must be immediately taken from the capacitor and sent to the grid, Figure 3.6(a).

- In the second part of the test, the full grid power is reversed, resulting in 600 W now being drawn from the grid into the converter. Average power flow to the capacitor must still be kept at zero, therefore, the power coming from the grid must be transferred at HF through the transformers from secondary to primary. The power drawn by the 50-Hz RL load is kept constant at 670 W. Under this new operating point, the dc supply only has to provide 70 W of the 670 W consumed by the load, because the grid is also supplying power to the system, Figure 3.6(b).

3.4.2 Results

The three-phase currents for both ac ports during part one of the test can be observed in the first half of the scope waveforms in Figure 3.7(a). Measurement of the phase-a transformer winding currents shows that they contain both HF (2 kHz) and LF (50 and 60 Hz for the primary and secondary windings, respectively) components, Figure 3.7(b), corresponding to DM and CM currents, respectively. According to Figure 3.3, the LF currents $\vec{\imath}_g'/2$ flowing through both halves of the secondary windings add up to the total ac current $\vec{\imath}_g'$ sent to the corresponding ac port, which consists of a high-quality LF current of 60 Hz. The same applies to the primary-side, where the LF currents $\vec{\imath}_g/2$ flowing through both halves of the primary windings add up to the current $\vec{\imath}_g$ drawn by the load, which is a high-quality 50-Hz current.

Analysis of the waveforms in the zoomed-in portion of Figure 3.7(b) reveals that the HF currents of both half-windings are in opposite directions. If we refer back to the diagram of the multiport converter (Figure 3.1), we can see that this is due to how the winding current direction is defined and confirms that the HF currents circulate in one direction, from one VSC to the other, as indicated in Figure 3.3.

Observing the second half of the current waveforms in Figure 3.7(a), once the grid power has been commanded to change direction, we can see that the current to the grid $\vec{\imath}_g'$ is reversed, while the RL load currents $\vec{\imath}_g$ remain unaltered by this diametrical change in power. This proves that the power between ac ports is completely decoupled.

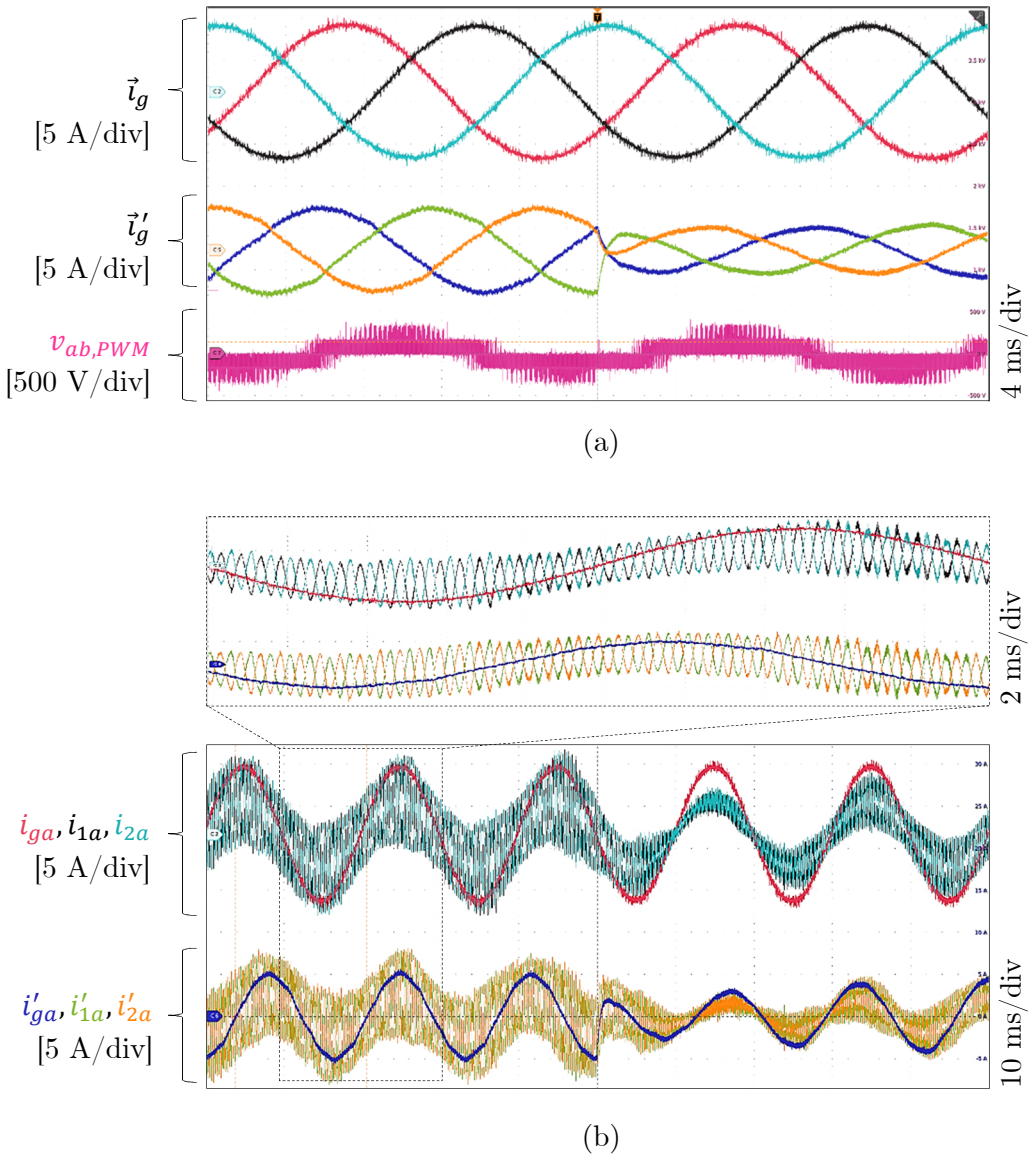

Figure 3.7. Experimental waveforms with power reversal on the 60-Hz grid. (a) Three-phase ac port currents and PWM line voltage. (b) Transformer winding currents overlaid on the two ac-port currents for one phase.

To maintain the voltage of the secondary dc port, the HF current must also be reversed, so that the instantaneous power coming from the grid and stored as charge in the capacitor is removed from it and transferred through the transformer to the primary side. This happens approximately 20 ms after the grid current is reversed: the amplitude of the HF component of the winding currents (i'_{1a} and i'_{2a}) in Figure 3.7(b) decreases, reversing at its lowest, before increasing again to maintain power balance among ports. Hence, the controller is able to decouple the dynamics of this dc port, by actively controlling the HF power flow through the transformers.

An additional benefit of the multiport converter is revealed in the waveform of the line voltage ($v_{ab,PWM}$), measured before the output filter. Different from the three-level PWM line voltage produced by a 2-L VSC (as in [18]; Table 1.1), this topology produces a five-level waveform. In addition, the frequency of the PWM line voltage is four times the switching frequency. As a comparison, a 2-L VSC generates a line voltage with PWM frequency of two times the switching frequency. Moreover, the leakage inductance of the windings contributes to the output inductance of the ac ports: analyzing the path of the grid currents ($\vec{\imath}_g$ and $\vec{\imath}_g'$) in Figure 3.3, it can be seen that the grid currents flow in parallel through each half winding before reaching the output inductance (L_{ac} and L_{ac}'). This results in an added inductance of $L_{eq}/8$. In summary, considering these advantages, the ac-port filtering requirements are reduced in this multiport converter.

3.5 Summary

By introducing center-tap terminals on the primary-side windings of the dc to ac converter an additional ac port is made available, resulting in a multiport converter with two dc and two ac ports. CM and DM voltages are generated on both sides of the transformer extending the multi-frequency modulation scheme presented for the dc to ac converter. This scheme superposes high-frequency DM signals (2 kHz) on two independent low-frequency CM signals (50 and 60 Hz). The HF ac sinusoidal DM currents flow between VSCs and are responsible for power transfer through the transformers. On each side of the transformers, the respective common-mode LF currents flow in parallel from the VSCs to the corresponding ac port. Parallel processing of the LF ac currents mitigates the conduction losses.

Three dq-frame current controllers operating at different frequencies are used: a HF current controller operating at 2 kHz is in charge of supervising power through the transformer; a LF controller operating at 50 Hz controls active power to a standalone three-phase load; a LF controller synchronized with the 60-Hz ac grid sets the desired active and reactive power. A dc supply is connected to the primary-side dc ports and a capacitor to the secondary-side dc port. A voltage PI controller keeps the capacitor charge constant.

Bidirectional dynamic performance is demonstrated with results from a 1.3-kW experimental prototype. The converter supplies constant power to a 50-Hz standalone three-phase load while

power to the 60-Hz grid is reversed. No disturbances appear on the 50-Hz ac currents in spite of the drastic change in the grid power. Complete power decoupling is thus demonstrated between ac ports.

Line voltage waveforms measured before the filter inductors reveal that the converter generates five-level PWM line voltages with four times the switching frequency. As a result, the converter has superior current quality and lower ac filtering requirements than multi-stage converter solutions that employ 2-L VSC stages.

Chapter 4

Conclusion

This thesis describes two converter systems that share a common magnetic and topological structure: a dc to ac converter and a multiport converter. Each of them can find applications in different settings. The research work presented here contributes to the state of the art in single-stage converters that offer HF isolation. This is a research area of power electronics whose goal is to investigate isolated topologies with high power density. An overwhelming amount of attention has been placed in the research literature on DAB-based converters, leaving other structures and operating principles unexplored. The topologies studied in this work have radically different operating and control principles from DAB-based converters, providing some important advantages.

A summary of the key findings that stem from the literature review and the simulation and experimental tests on both converters is presented in this concluding chapter, followed by a discussion on different research paths and work extensions that have been opened by studying these converters.

4.1 Summary

The inclusion of transformers is a requirement of power converters in several applications. Converters that integrate transformers offer galvanic separation, voltage matching and dc blocking capabilities. However, transformers can be one of the heaviest and bulkiest elements of power converters, especially at low frequencies. Operating them at higher frequencies allows for considerable reductions in both size and weight. For this reason, it is very common to find HF transformers in isolated power converters.

Practically, almost all HF isolated converters interact with either dc or LF ac systems, and not with systems operating at the frequency of the transformers. Therefore, converters must be able to generate the appropriate dc or LF ac currents and voltages at their input and output ports, regardless of the frequency used for the operation of the HF transformers. The traditional solution has been to use multiple cascaded converter stages. This, however, can result in increased number of components, translating in higher cost, losses, and reduced power density. Consequently, research has been carried out to further increase the power density of HF isolated converters by using a single conversion stage.

Most single-stage converters with HF isolation are based on the DAB principle of operation, due to the inherent advantages of this converter: possibility to operate the transformer at the switching frequency, minimizing its size and weight, noncomplex control, and the possibility to use soft commutation to increase efficiency at high switching frequencies. Yet, some drawbacks of DABs are the nonlinear relation between power and the phase-shift angle, which adds complexity to the derivation of controllers, as well as the increasing reactive currents in the transformer windings for higher phase-shift angles. Moreover, a disadvantage specific to single-stage converters using the DAB principle is the dependence of the maximum transformer power transfer with the duty ratio of the square-wave voltages, which, when used as a control variable, moves away from 50% duty (i.e., from perfect square-wave pulses) limiting how much power can be sent through the transformer. In the case of multiport converters, no single-stage solutions with HF isolation were found in the published literature that could achieve ac-ac power conversion.

The converters presented in this thesis achieve HF power transfer and control of dc and LF ac ports using a multi-frequency PWM modulation strategy that takes advantage of the independent nature of DM and CM voltages and currents that can exist in center-tapped transformers connected to dual inverters. The main takeaways of the converters are as follows:

- Experimental waveforms have proven that both converters use sinusoidal HF currents to send power through the transformers. It is for this reason that the HF currents can be directly controlled in dq-frame, making their implementation a straightforward task.
- The direct control of the currents ensures that no unnecessary reactive currents arise in the windings (HF voltages and currents are kept in phase).

- Maximum power through the transformers is not tied to the ac grid modulation depth, as with DAB-based converters. Therefore, HF and LF power are completely independent.
- Power reversal tests have shown that the independence of DM and CM domains and the closed-loop control strategies adopted ensure complete decoupling of the dynamics of the dc and ac ports of both converters.
- The steady-state and dynamic conditions experimentally presented for the multiport converter have proven that simultaneous operation of asynchronous three-phase ac ports can be achieved. This is a unique contribution, as no other HF-isolated single-stage multiport converters have been found in literature to offer asynchronous ac-ac conversion.
- Power through the transformer has redundant paths, increasing reliability. If a switching device fails, power through the transformer can still be sent using the unaffected phases. This is an advantage compared to reduced-switch-count multi-stage converters that employ a single-phase DAB stage.
- Experimental PWM line voltage waveforms show that the converters offer higher current quality than 2-L VSCs, which are used in multi-stage converters. Tied to the filtering action of the leakage inductance of the windings, this results in lower ac filtering requirements.
- Analysis of the experimental winding current waveforms confirm the DM and CM current paths of the converters. LF ac currents are, thus, processed in parallel, which reduces the conduction losses, compared to multi-stage converters that use 2-L VSCs to interface with the grid.

In spite of these advantages, the converters presented here have some challenges that give an edge in some areas to its main competitors, namely, DAB-based converters and multi-stage converters:

- First of all, no soft switching is considered in this work, therefore converters using the DAB principle (both single and multi-stage) have the advantage of reduced switching losses.
- Multi-stage converters using a single-phase DAB stage have a lower active switch count, potentially reducing cost and complexity, while increasing power density.

- Although the converters presented in this work use HF power transfer, the fact that DAB-based converters can operate the transformers at the switching frequency means that they can further reduce the transformer weight and size.
- Operating the HF transformers at frequencies close to the audible range pose a challenge in terms of noise emission. This is not the case for DAB-based converters operating at the switching frequency, which is well beyond the human audible spectrum. Although the frequency of the presented converters can be chosen to be higher to solve this problem, this will result in increased switching frequency requirements and, also, the impedance of the transformers at this new HF will have to be taken into consideration.
- It has been discussed that to synthesize both the HF and LF components employed in the multi-frequency modulation scheme, a higher dc voltage is required, compared to converters that use the DAB principle.

To ease comparison, the areas where the presented converters and the main alternatives published in literature have the edge are summarized below.

Table 4.1. Qualitative comparison of converters. [a]

	Multi-stage converters [b]	DAB-based converters [c]	Multiport converter	DC-AC converter
Control linearity	+	+	−	−
Reactive winding currents	+	+	−	−
Decoupled HF and LF power	+	+	−	+
HF power transfer reliability (redundancy)	+	+	+	−
AC filtering requirements (current quality)	+	+	ND	−
Conduction losses (parallel current processing)	+	+	+	−
Commutation losses (soft switching)	−	−	+	=
Active switch count	=	=	=	+
Transformer size and weight	−	−	+	+
Audible noise	−	−	+	+
DC rail voltage requirement	−	−	+	+

[a] Symbol legend: (+) At advantage; (−) At disadvantage; (=) Same; (ND) Not determined.
[b] Converters [26] and [18] are considered here for the multi-stage converter category (Table 1.1).
[c] Converters [28] and [35] are considered here for the DAB-based converter category (Table 1.1).

4.2 Future Work

The research work reported in this document has reached the stage of concept validation, where experimental results have confirmed the theoretical analysis. As such, it is natural that the research direction that comes after is mainly concerned with the following areas:

- Design optimization: Equations should be derived to relate the main design parameters of the components of both converters with the power, voltage, and current ratings of the applications where the converters are of most value. This will involve the design of the HF transformers, filters, dc voltage levels, the frequency of the transformers and the ratio of the modulation depth assigned to the HF and LF components (defined by m'_{HFd}), as well as the selection of the appropriate switching devices.
- Loss analysis: Using an optimal design, simulations should be carried out to analyze the switching and conduction losses of commutation devices, copper and iron losses in the transformers, heating losses in the wiring and dc capacitor losses. Efficiency curves can be then generated at different power levels. An optimized experimental prototype can validate the simulated efficiency of the converter.
- Efficiency comparison: During the review process of the publications mentioned in the preface, reviewers have shown interest in comparing the efficiency of the converters with multi-stage converters using single-phase DABs, as they have a lower switch count and provide soft switching in the DAB stage. These multi-stage converters can be simulated using similar parameters to give a direct comparison.
- Switch stress analysis: Peak voltages and currents seen by the switches should be analyzed. The switch utilization factor could be derived to provide a fair point of comparison with other topologies.
- Electromagnetic interference (EMI) assessment: The use of loose coupling between transformer windings helps to limit the switch-mode reactive currents flowing through them, but this may pose a challenge in terms of EMI. An analysis would be desirable to determine if this may pose a problem and, if so, to be in better position to come up with solutions.

- Decoupling capacitance reduction: Simulations with the dc to ac converter have shown that the capacitance for a 10-kW converter can be made sufficiently small to use a film capacitor if the bandwidth of the capacitor voltage controller is increased. However, experimentally, increasing this bandwidth has been challenging, likely due to noise feedback. Efforts could be made to improve the controller design or reduce noise interference in the control path.

In addition, there are some topological variations and application scenarios that would be of interest to investigate, expanding the principles that have been presented in this work:

- WECS application: The multiport converter has been suggested as a candidate for wind energy applications with integrated battery storage and voltage step up. This can be demonstrated in simulations and experimentally, running a generator in the laboratory. Some high-level decisions involving the goals of the main controllers would have to be made and field-oriented control should be used for the generator-side ac port.
- Fault tolerance: It is also suggested that for a specific application of each of the two converters, typical fault scenarios are simulated and analyzed to determine further strengths and challenges of these topologies. One of the scenarios that have been, by chance, observed experimentally in the dc to ac converter is that when one of the switches fail, power can still be sent through the transformers without disrupting the operation of the converters. More advantages like this could be discovered by analyzing fault scenarios.
- To reduce the switch count, a couple of variations are suggested as future work, namely:
    - For the dc to ac converter, a suggestion is to substitute the primary-side VSC2 with a wye connection. This would eliminate six active switches but will likely come at the expense of higher primary-side dc voltage requirement, as opposing HF voltages could no longer be impressed across the windings.
    - For the multiport converter, an asymmetric version could be proposed to further increase power density and compete against low-switch-count topologies. It would use a single transformer core and dual inverter legs for only one of the phases (e.g., for phase A), eliminating 8 active switches and two transformers. The modulation would be almost the same, except that only one of the inverter

legs (both at the primary and secondary sides) would be modulated with both the LF and HF signals, whereas the remaining inverter legs would only need the LF modulating signal.

Bibliography

[1] B. Brooks and S. White, PV and the NEC, New York: Routledge Taylor & Francis Group, 2018.

[2] Deutsche Gesellschaft für Sonnenenergie, Planning and Installing Photovoltaic Systems: A Guide for Installers, Architects and Engineers, New York: Routledge Taylor & Francis Group, 2013.

[3] Emilio and M. D. Paolo, "Galvanic Isolation in EV and HEV Applications," EE Times, 11 March 2020. [Online]. Available: https://www.eetimes.eu/galvanic-isolation-in-ev-and-hev-applications/. [Accessed 11 July 2021].

[4] ABB, "Drives," 2021. [Online]. Available: https://new.abb.com/drives. [Accessed 12 July 2021].

[5] D. Xu, F. Blaabjerg, W. Chen and N. Zhu, Advanced Control of Doubly-Fed Induction Generator for Wind Power Systems, Hoboken, New Jersey: John Wiley & Sons, Inc., 2018.

[6] T. Wildi, Electrical Machines Drives and Power Systems, Harlow, Essex: Pearson Education Limited, 2014, pp. 601-674.

[7] J. W. Kolar, T. Friedli, J. Rodriguez and P. W. Wheeler, "Review of Three-Phase PWM AC–AC Converter Topologies," *IEEE Transactions on Industrial Electronics,* vol. 58, no. 11, pp. 4988-5006, 2011.

[8] ABB, "Active Front End Drive Technologies," 13 May 2019. [Online]. Available: https://library.e.abb.com/public/c8af953d75f74a4cbea2f8bfde2099a7/LVD-PNTN19U-EN_REVA.pdf. [Accessed 13 July 2021].

[9] R. Kawashima, T. Mishima and C. Ide, "Three-Phase to Single-Phase Multiresonant Direct AC–AC Converter for Metal Hardening High-Frequency Induction Heating Applications," *IEEE Transactions on Power Electronics,* vol. 36, no. 1, pp. 639-653, 2021.

[10] P. S. Huynh, D. Ronanki, D. Vincent and S. S. Williamson, "Direct AC–AC Active-Clamped Half-Bridge Converter for Inductive Charging Applications," *IEEE Transactions on Power Electronics,* vol. 36, no. 2, pp. 1356-1365, 2021.

[11] F. H. Ahmed, M. S. El Moursi, B. Zahawi and K. Al Hosani, "A High-Frequency Isolated Multilevel Cascaded-Type Bipolar Direct PWM AC–AC Converter for Utility Voltage Compensation," *IEEE Transactions on Industry Applications,* vol. 57, no. 3, pp. 3188-3201, 2021.

[12] A. Olloqui, J. L. Elizondo, M. Rivera, M. E. Macías, O. M. Micheloud, R. Peña and P. Wheeler, "Model-Based Predictive Rotor Current Control Strategy for Indirect Power

Control of a DFIM Driven by an Indirect Matrix Converter," *IEEE Transactions on Energy Conversion,* vol. 36, no. 2, pp. 1510-1516, 2021.

[13] General Electric Company, "GCCIA Phase 1: Making Interconnection in the Gulf a Reality," 2018. [Online]. Available: https://www.gegridsolutions.com/products/applications/hvdc/gccia-interconnection-brochure-en-2018-05-grid-pea-0570.pdf. [Accessed 14 July 2021].

[14] S. Bhattacharya, "Smart Transformers Will Make the Grid Cleaner and More Flexible," 29 June 2017. [Online]. Available: https://spectrum.ieee.org/energy/renewables/smart-transformers-will-make-the-grid-cleaner-and-more-flexible. [Accessed 13 July 2021].

[15] J. I. Leon, E. Dominguez, L. Wu, A. Marquez Alcaide, M. Reyes and J. Liu, "Hybrid Energy Storage Systems: Concepts, Advantages, and Applications," *IEEE Industrial Electronics Magazine,* pp. 74-88, March 2021.

[16] M. Chen and H. V. Poor, "High-Frequency Power Electronics at the Grid Edge: A Bottom-Up Approach Toward the Smart Grid," *IEEE Electrification Magazine,* pp. 6-17, September 2020.

[17] A. K. Bhattacharjee, N. Kutkut and I. Batarseh, "Review of Multiport Converters for Solar and Energy Storage Integration," *IEEE Transactions on Power Electronics,* vol. 34, no. 2, pp. 1431-1445, 2019.

[18] J. Ge, Z. Zhao, L. Yuan and T. Lu, "Energy Feed-Forward and Direct Feed-Forward Control for Solid-State Transformer," *IEEE Transactions on Power Electronics,* vol. 30, no. 8, pp. 4042-4047, 2015.

[19] D. K. Mishra, M. J. Ghadi, L. Li, M. J. Hossain, J. Zhang, P. K. Ray and A. Mohanty, "A review on solid-state transformer: A breakthrough technology for future smart distribution grids," *International Journal of Electrical Power and Energy Systems,* vol. 133, pp. 1-15, 2021.

[20] F. Jauch and J. Biela, "An innovative bidirectional isolated multi-port converter with multi-phase AC ports and DC ports," in *European Conference on Power Electronics and Applications (EPE)*, Lille, France, 2013.

[21] G. Neidhöfer, "50-Hz Frequency [History]," *IEEE Power and Energy Magazine,* pp. 66-81, July 2011.

[22] H. Hu and Y. Xing, "Design Considerations and Fully Digital Implementation of 400-Hz Active Power Filter for Aircraft Applications," *IEEE Transactions on Industrial Electronics,* vol. 61, no. 8, pp. 3823-3834, 2014.

[23] S. J. Chapman, Electric Machinery Fundamentals, New York: McGraw-Hill, 2012.

[24] Metglas, Inc., "Amorphous Alloys for Transformer Cores," 29 April 2011. [Online]. Available: https://metglas.com/wp-content/uploads/2021/06/2605SA1-Magnetic-Alloy-Updated.pdf. [Accessed 17 July 2021].

[25] Gaotune Technologies Co., Ltd., "Amorphous C-Core," 2021. [Online]. Available: http://www.gaotune.com.hk/amorphous-core/c-core/amorphous-c-core-7.html. [Accessed 17 July 2021].

[26] S. Inoue and H. Akagi, "A Bidirectional DC–DC Converter for an Energy Storage System With Galvanic Isolation," *IEEE Transactions on Power Electronics,* vol. 22, no. 6, pp. 2299-2306, 2007.

[27] L. A. Ramos, R. F. Van Kan, M. Mezaroba, A. L. Batschauer and C. Rech, "A Bidirectional Single-Stage Isolated AC-DC Converter for Electric Vehicle Chargers," in *IEEE Energy Conversion Congress and Exposition (ECCE)*, Baltimore, MD, USA, 2019.

[28] B. R. Almeida, J. W. M. Araújo, P. P. Praça and D. S. Oliveira, "A Single-Stage Three-Phase Bidirectional AC/DC Converter With High-Frequency Isolation and PFC," *IEEE Transactions on Power Electronics,* vol. 33, no. 10, pp. 8298-8307, 2018.

[29] S. Chakraborty and S. Chattopadhyay, "A Dual-Active-Bridge-Based Novel Single-Stage Low Device Count DC–AC Converter," *IEEE Transactions on Power Electronics,* vol. 34, no. 3, pp. 2339-2354, 2019.

[30] Y. P. Chan, K. H. Loo and Y. M. Lai, "Single-Stage Resonant AC-DC Dual Active Bridge Converter with Flexible Active and Reactive Power Control," in *IEEE Vehicle Power and Propulsion Conference*, Hangzhou, China, 2016.

[31] B. Koushki, P. Jain and A. Bakhshai, "A bi-directional AC-DC converter for electric vehicle with no electrolytic capacitor," in *IEEE International Symposium on Power Electronics for Distributed Generation Systems*, Vancouver, 2016.

[32] D. Ma, W. Chen, L. Shu, X. Qu and K. Hou, "A MMC-Based Multiport Power Electronic Transformer With Shared Medium-Frequency Transformer," *IEEE Transactions on Circuits and Systems II: Express Briefs,* vol. 68, no. 2, pp. 727-731, 2021.

[33] H. S. Krishnamoorthy, D. Rana, P. Garg, P. N. Enjeti and I. J. Pitel, "Wind Turbine Generator–Battery Energy Storage Utility Interface Converter Topology With Medium-Frequency Transformer Link," *IEEE Transactions on Power Electronics,* vol. 29, no. 8, pp. 4146-4155, 2014.

[34] K. Itoh, M. Ishigaki, N. Yanagizawa, S. Tomura and T. Umeno, "Analysis and Design of a Multiport Converter Using a Magnetic Coupling Inductor Technique," *IEEE Transactions on Industry Applications,* vol. 51, no. 2, pp. 1713-1721, 2015.

[35] A. U. Barbosa, B. R. Almeida, D. S. Oliveira, P. P. Praça and L. H. Barreto, "Multi-port bidirectional three-phase AC-DC converter with high frequency isolation," in *2018 IEEE*

Applied Power Electronics Conference and Exposition (APEC), San Antonio, TX, USA, 2018.

[36] A. K. Bhattacharjee and I. Batarseh, "An Interleaved Boost and Dual Active Bridge Based Single Stage Three Port DC-DC-AC Converter With Sine PWM Modulation," *IEEE Transactions on Industrial Electronics,* vol. 68, no. 6, pp. 4790-4800, 2021.

[37] J. Khodabakhsh and G. Moschopoulos, "Simplified Hybrid AC–DC Microgrid With a Novel Interlinking Converter," *IEEE Transactions on Industry Applications,* vol. 56, no. 5, pp. 5023-5034, 2020.

[38] Infineon Technologies AG, "(H)EV on-board battery charger - hybrid / electric vehicle," 2021. [Online]. Available: https://www.infineon.com/cms/en/applications/automotive/electric-drive-train/onboard-battery-charger/. [Accessed 19 July 2021].

[39] The Railway Technical Website, "Electric Locomotives," 2019. [Online]. Available: http://www.railway-technical.com/trains/rolling-stock-index-l/electric-locomotives/. [Accessed 19 July 2021].

[40] S. A. Gorji, H. G. Sahebi, M. Ektesabi and A. B. Rad, "Topologies and Control Schemes of Bidirectional DC–DC Power Converters: An Overview," *IEEE Access,* vol. 7, pp. 117997-118019, 2019.

[41] W. M. Santos, "Estudo e implementação do conversor TAB (Triple Active Bridge) aplicado a sistemas renováveis solares fotovoltaicos," Florianopolis, Brazil, 2011.

[42] Texas Instruments Inc., "Power Supply Design Seminar: Survey of Resonant Converter Topologies," 2018. [Online]. Available: https://www.ti.com/seclit/ml/slup376/slup376.pdf. [Accessed 21 May 2021].

[43] B. R. Almeida, "Conversor CC-CA de único estágio, bidireccional isolado em alta frequência com correcao de fator de potência," Federal University of Ceara, Fortaleza, Brazil, 2016.

[44] A. Yazdani and R. Iravani, Voltage-sourced converters in power systems: modeling, control and applications, Hoboken, NJ: John Wiley & Sons, 2010.

[45] T. Friedli and J. W. Kolar, "Milestones in Matrix Converter Research," *IEEJ Journal of Industry Applications,* vol. 1, no. 1, pp. 2-14, 2012.

[46] D. F. Menzies, J. Graham and F. Uchoas Ribeiro, "“Garabi” the Argentina – Brazil 1000 MW Interconnection Commissioning and Early Operating Experience," June 2001. [Online]. Available: https://library.e.abb.com/public/336dd56474cadec5c1256fda004aeadd/Erlac01.pdf. [Accessed 14 July 2021].